JOURNAL OF CHEMICAL INFORMATION AND MODELING

Article

pubs.acs.org/jcim

Experimentally Guided Structural Modeling and Dynamics Analysis of Hsp90−p53 Interactions: Allosteric Regulation of the Hsp90 Chaperone by a Client Protein

Kristin Blacklock[†] and Gennady M. Verkhivker*[,†,‡]

[†]School of Computational Sciences and Crean School of Health and Life Sciences, Schmid College of Science and Technology, Chapman University, One University Drive, Orange, California 92866, United States

[‡]Department of Pharmacology, University of California San Diego, 9500 Gilman Drive, La Jolla, California 92093, United States

Supporting Information

ABSTRACT: A fundamental role of the Hsp90 chaperone system in mediating maturation of protein clients is essential for the integrity of signaling pathways involved in cell cycle control and organism development. Molecular characterization of Hsp90 interactions with client proteins is fundamental to understanding the activity of many tumor-inducing signaling proteins and presents an active area of structural and biochemical studies. In this work, we have probed mechanistic aspects of allosteric regulation of Hsp90 by client proteins via a detailed computational study of Hsp90 interactions with the tumor suppressor protein p53. Experimentally guided protein docking and molecular dynamics structural refinement have reconstructed the recognition-competent states of the Hsp90−p53 complexes that are consistent with the NMR studies. Protein structure network analysis has identified critical interacting networks and specific residues responsible for structural integrity and stability of the Hsp90−p53 complexes. Coarse-grained modeling was used to characterize the global dynamics of the regulatory complexes and map p53-induced changes in the conformational equilibrium of Hsp90. The variations in the functional dynamics profiles of the Hsp90−p53 complexes are consistent with the NMR studies and could explain differences in the functional role of the alternative binding sites. Despite the overall similarity of the collective movements and the same global interaction footprint, p53 binding at the C-terminal interaction site of Hsp90 may have a more significant impact on the chaperone dynamics, which is consistent with the stronger allosteric effect of these interactions revealed by the experimental studies. The results suggest that p53-induced modulation of the global dynamics and structurally stable interaction networks can target the regulatory hinge regions and facilitate stabilization of the closed Hsp90 dimer that underlies the fundamental stimulatory effect of the p53 client.

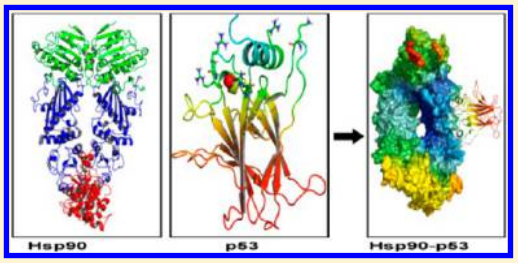

INTRODUCTION

The molecular chaperone Hsp90 (90 kDa heat-shock protein) plays a central role in the biogenesis and activation of many client proteins by assisting in the initial folding of the polypeptide chain and protecting activation-competent protein states from degradation and aggregation.[1−5] Fundamental understanding of the Hsp90 mechanisms at the molecular level is one of central objectives in cancer biology because major hallmarks of cancer[6] can be simultaneously targeted by disruption of the Hsp90 machinery. Hsp90 is highly conserved in a variety of organisms and is essential for the integrity and viability of signaling pathways involved in cell cycle control and organism development. The assembly and activation of many signaling proteins, including hormone receptors, transcription factors, and protein kinases, are under the control of Hsp90.[7−14] A dynamic process of loading and release of client proteins to the Hsp90 chaperone is supported by cochaperones that modulate the ATPase-coupled conformational changes tailored for structural and functional requirements of the protein clientele. Structural versatility of Hsp90 cochaperones is utilized by the chaperone machinery in inhibition and activation of the ATP hydrolysis, modulation of conformational flexibility, and recruitment of specific protein clients to Hsp90.[12−14] A general mechanism involves cochaperone-mediated client recruitment to the Hsp90−cochaperone machinery via transient regulatory complexes, upon which the mature protein can be released following a cell signal that is coupled to the conformational changes of Hsp90 and ATP hydrolysis. Allosteric targeting of the Hsp90 clients by disabling cochaperone binding has emerged as a novel strategy for discovery of anticancer agents.[15−18] The interruption of protein client binding leaves the Hsp90 activity unaffected, whereas specific client proteins could be selectively inhibited by being prevented from binding to the Hsp90 machinery.

The abundance of structural and functional data has vastly improved our understanding of the underlying chaperone mechanisms.[19−21] A conserved modular architecture of Hsp90 consists of three well-defined domains: an N-terminal domain (Hsp90-N) responsible for ATP binding, a middle domain

Received: July 24, 2013
Published: November 5, 2013

(Hsp90-M), which completes the ATPase site and binds client proteins, and a C-terminal domain (Hsp90-C) that is required for dimerization (Figure 1). Structural studies have determined

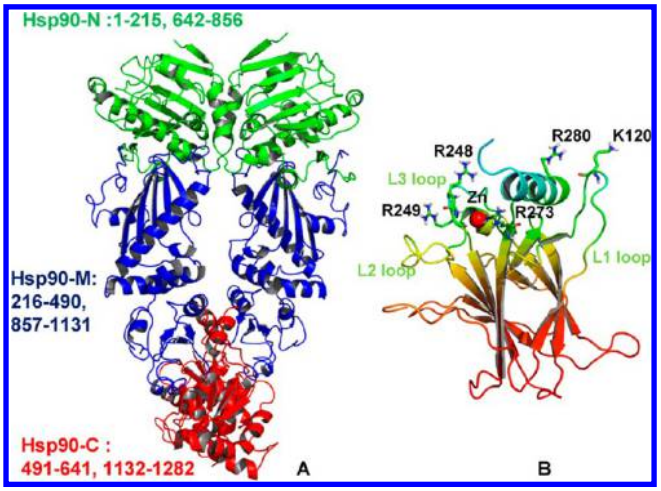

Figure 1. Structures of the Hsp90 dimer (A) and p53-DBD (B). The homodimer architecture of the full-length Hsp9p0 dimer is illustrated by the crystal structure of a closed conformation of yeast Hsp90 dimer.[22] The structure is shown in a ribbon representation with a detailed annotation of the Hsp90-N domain (green), Hsp90-M domain (blue), and Hsp90-C domain (red). A representative conformation of the p53-DBD from the NMR ensemble of solution structures is shown (B). The key structural motifs and DNA recognition residues of the p53-DBD are indicated and shown in bold sticks.

that Hsp90 can assume a variety of distinct structural forms associated with the ATP binding and hydrolysis.[22−26] Recent biophysical studies using hydrogen exchange mass spectrometry (HX-MS), electron microscopy (EM), and small-angle X-ray scattering (SAXS), as well as ensemble and single molecule fluorescence resonance energy transfer (FRET) assays have provided a detailed characterization of the Hsp90 conformational states.[27−31] According to these studies, in the absence of cochaperones and substrate proteins, the Hsp90−ATPase cycle is a stochastic switch operating via spontaneous conformational transitions between different functional states.[29−31] Conformational changes of Hsp90 may be only weakly coupled to nucleotide binding,[29] and the Hsp90−ATPase cycle is driven by thermal fluctuations.[31] Binding of cochaperones can shift the conformational equilibrium of Hsp90 into a specific succession of states, thus providing spatial and temporal directionality to the ATPase cycle.[29−31] While in its isolated form, Hsp90 has a weak ATPase activity,[32,33] the interactions of Hsp90 with its various cochaperones can differentially modulate the progression of the ATPase cycle and allow for timely coordination of the loading, activation, and release of client proteins.[34,35] To facilitate the completion of the ATPase cycle, Hsp90 associates with Aha1 (activator of heat shock 90 kDa protein ATPase homologue 1), which is the only known cochaperone that markedly stimulates the ATPase activity.[36,37] The regulatory role of the Hsp90 interactions with its cochaperone Aha1 is crucial for modulation and progression of the Hsp90−ATPase cycle by biasing Hsp90 toward an N-terminally dimerized state preceding the catalytically active closed state.[38−42] The stimulatory effect on the Hsp90−ATPase activity and stabilization of specific Hsp90 conformations may be enhanced through binding with the client proteins, including the glucocorticoid receptor,[33] staphylococcal nuclease,[43] ribosomal protein L2,[44] and α-synuclein.[45] The interactions of Hsp90 with cochaperones and client proteins are dynamic and often synergistic in nature, causing cooperative structural changes in the interacting partners and allosterically influencing global conformational rearrangements of Hsp90.[46−49] Large scale proteomics studies have revealed evolutionary and structural diversity of the Hsp90 clientele.[50−54] According to these studies, the critical determinants that control recognition and recruitment of client proteins to the Hsp90 machinery include (a) preferential binding to the clients that are only marginally stable in their native folds and (b) client-induced conformational changes and stabilization of specific Hsp90 conformations that result in stimulation of Hsp90−ATPase activity.[50]

Among a diverse spectrum of Hsp90 client proteins, p53 is of special therapeutic importance as this protein functions as a tumor suppressor and is mutated in more than 50% of human cancers, rendering many cancer-altered networks to become dependent on the Hsp90−p53 machinery.[55] The core domain of tumor suppressor p53 (residues 94−312) is marginally stable and prone to conformational changes at elevated temperatures that determines the overall functional activity of the full-length protein,[55−58] including inactivation in 50% of human cancers by oncogenic mutations mostly found in the DNA binding core domain of p53 (p53-DBD).[56,59] The structure of the p53-DBD consists of a central β-sandwich scaffold and structural elements that form the DNA-binding surface, which include a loop-sheet-helix motif and two large loops L2 and L3 (Figure 1). NMR spectroscopy determination of the p53 core domain structure in solution has revealed the intrinsic instability of p53 that on the structural level is manifested in structural plasticity of the hydrophobic core.[60] These studies have concluded that the p53 core domain may have evolved to be marginally stable at physiological temperatures to allow for a spontaneous denaturation of p53. The p53 protein can be activated by Hsp90,[61−63] and the tumor suppressor binding to the DNA promoter sequence is Hsp90-dependent as the molecular chaperone is required to support the transcriptional activity of p53 in cells.[64−67] Recent reports have suggested a mechanism of Hsp90-mediated regulation of the p53-DNA binding, according to which Hsp90 is capable of folding wild type (WT) p53 protein.[66] These studies have determined that the p53-DBD as a minimal region required for binding with Hsp90, whereas both the Hsp90-M and Hsp90-C domains could be engaged in binding with the client protein.[66] Biochemical affinity assays have initially suggested that binding of the p53-DBD to the Hsp90-M domain could be stronger than to the Hsp90-C domain.[66] Hsp90-assisted p53 folding appeared to be essential for restoring cellular functions and stabilization of mutated p53 variants but not for stabilization and activation of the p53-WT.[67] It was also suggested that Hsp90 binds p53 in native or nearly native conformation.[68] According to an alternative mechanism, binding of Hsp90 may induce conformational changes resulting in partial unfolding of p53, and the ATP-driven dissociation of the Hsp90−p53 complex could stimulate refolding of p53 to an active conformation that may prevent p53 aggregation and facilitate p53 binding to the promoter sequence.[64,69]

The initial NMR analysis of the p53-DBD interactions with human Hsp90 has indicated that heat-treated p53 may be partially unfolded in the complex.[70] The p53 core domain may adopt non-native, molten, globule-like conformations under mild denaturing conditions, such as incubation at moderately

low pH.[71] The recent NMR analysis supported by hydrogen exchange and fluorescence experiments has evidenced a dynamic manifold of conformational states resembling a molten globule-like state that may be formed by the p53 DNA-binding domain in the presence of the Hsp90-N and Hsp90-M domains.[72] The dynamic and nonspecific nature of the p53 interactions with multiple domains of Hsp90 was further evidenced in another NMR study of this group.[73] Nevertheless, this investigation has also pointed to the dominant intermolecular interface on Hsp90 that involves proximity of the Hsp90-N and the Hsp90-M domains. Structure−functional studies have also strongly supported a mechanism in which the folded form of the p53-DBD would interact with the Hsp90 dimer. NMR spectroscopy experiments and biophysical methods have identified the p53-DBD interacting sites at both Hsp90-M and Hsp90-C domains that could mediate interactions with the folded yet highly flexible form of the p53-DBD.[74] Binding of p53 can also potentiate the stimulatory effect of the cochaperone Aha1 suggesting a synergistic function of these proteins in enhancing the ATPase activity.[74]

Structural studies of the Hsp90−client interactions using EM, SAXS, and NMR approaches have produced thus far low resolution information about Hsp90 complexes with only three client proteins: staphylococcal nuclease,[43] p53 protein,[74] and cyclin-dependent kinase 4 (Cdk4).[75] The dynamic nature of Hsp90 complexes can often hinder the molecular details underlying modulation of the Hsp90 interactions in the regulatory complexes. Multi-scale approaches that combine protein−protein docking with all-atom molecular dynamics (MD) simulations and coarse-grained modeling of the equilibrium complexes can be used to probe client-induced changes in structural stability of the interacting networks and quantify the global dynamics of the chaperone. A combination of MD simulations and the protein structure network (PSN) analysis using a graph-based representation of the residue interactions can identify functionally important sites and subtle structural changes in the conformational populations of states.[76−83] Graph-based protein networks that incorporated dynamic contact maps of cross-correlations with the interaction residue connectivity have successfully described allosteric communications in tRNA−protein complexes,[84] cysteinyl tRNA synthetase,[85,86] imidazole glycerol phosphate synthase,[87,88] thrombin,[89] and the M2 muscarinic receptor.[90] Functional dynamics and collective protein motions are largely determined by the native interactions and low frequency normal modes of fluctuations around the equilibrium structure. Although principal modes of protein motions can be extracted from all-atom MD simulations, coarse-grained approaches and elastic network models (ENM) such as the Gaussian network model (GNM)[91−94] combined with the normal-mode analysis (NMA)[96,96] are far more efficient and often more accurate[97−99] in probing functional motions. Computational studies have employed these approaches to reveal the atomic details of the allosteric pathways that may regulate the conformational equilibrium of the Hsp90.[100−108] In this work, we combined experimentally guided protein docking and MD-based refinement of the Hsp90−p53 complexes with the graph-based network analysis to identify functionally important residues and interactions responsible for structural stability of the Hsp90 complexes with the p53-DBD. Coarse-grained modeling of the equilibrium Hsp90−p53 structures was employed to characterize the global dynamics of the regulatory complexes and map client-induced changes in the conformational equilibrium of Hsp90 upon p53 binding. A detailed quantitative analysis of the p53-induced conformational changes in Hsp90 at the global topology level and at the level of specific interactions complements NMR studies and provides additional insights into mechanistic aspects of allosteric regulation of Hsp90 by client proteins.

METHODS

Protein−Protein Docking. Our approach is based on the data-driven HADDOCK methodology[109−111] that integrates mutagenesis data and NMR chemical shift perturbations as experimental restraints in docking of protein complexes. We converted the experimental NMR data[74] into a series of ambiguous interaction restraints (AIR) to guide docking of the Hsp90−p53 complexes. The crystal structures of the full-length Hsp90 dimer were obtained from the Protein Data Bank (PDB) and included the crystal structure of yeast Hsp90 (PDB ID 2CG9),[22] crystal structures of the bacterial homologue HtpG in open free form (PDB ID 2IOQ) and ADP-bound form (PDB ID 2IOP),[23] and crystal structures of the mammalian Grp94 homologue in complexes with ADP (PDB ID 2O1V) and AMP-PNP (PDB ID 2O1U),[24] as well as solution structures of apo-HtpG obtained at high pH and low pH conditions.[25,26] The NMR ensemble of solution structures of the p53-DBD (PDB ID 2FEJ)[60] was used for the ensemble-based p53 docking. The structures were prepared for docking using the WHAT-IF online server.[112]

According to the NMR studies[74] a negatively charged amino acid stretch at the C-terminal that was not resolved in the crystal structure of a closed Hsp90 dimer (residues 680−689, PDB ID 2CG9) can mediate binding of the p53-DBD at the Hsp90-C domain. We have generated models of the unresolved C-terminal tail regions in Hsp90 using LOMETS,[113] a server for protein threading algorithms, and MUSTER,[114] a specific threading algorithm. A 35-residue sequence (675-GLNIDE-DEETETAPEASTAAPVEEVPADTEMEEVD-709) and a shorter 17-residue sequence (675-GLNIDEDEETETAPEAS-691) of the C-terminal tail were subjected to structural modeling using these tools. The protein threading programs generated 30 best scoring models for each sequence. The structurally unresolved stretch of residues 679−689 at the C-terminal tail showed high flexibility in the NMR experiments,[74] thus indicating the absence of any preferred secondary structure. On the basis of these criteria, we selected three best models for the larger sequence and one best model for a smaller sequence that lacked secondary structure, while they appeared to be precisely aligned with the last stretch of resolved Hsp90-CTD residues (674-LGLN-677) in the crystal structure (PDB ID 2CG9). In other words, the selected structures of the C-terminal tail did not compromise structural arrangement of the preceding residues in the crystal structure.

In the construction of AIRs data, we first defined the protein residues that could form the intermolecular Hsp90−p53 interface using the NMR chemical shift perturbation data.[74] The selection of active residues (Tables 1 and 2) is fully consistent with the definition adopted in the NMR analysis[74] by the Buchner group (see for comparison, Table 1, Supporting Information , from that study). In this selection, active residues were chosen based on significance of the chemical shifts, according to which all perturbations higher than the average are considered significant.[109−111] Active residues are the ones that were experimentally identified as involved in the Hsp90−p53 interactions and solvent accessible in the uncomplexed

Table 1. AIR Template for HADDOCK Simulations of Hsp90−p53 Complexes in Hsp90-M Binding Site

interaction	AIR template	Hsp90-M	P53
interaction 1	active residues	282−292	116−122, 138,175,184, 235−250, 272−285
interaction 2	active residues	305−308	116−122, 138, 175, 184, 235−250, 272−285
interaction 3	active residues	326	116−122, 138, 175, 184, 235−250 ,272−285
interaction 4	active residues	400−423	116−122, 138, 175, 184, 235−250, 272−285
interaction 5	active residues	445−464	116−122, 138, 175, 184, 235−250, 272−285
interaction 1	passive residues	272−288	123−141, 161−174, 185−198, 251−253, 270−290
interaction 1	passive residues	293−297	123−141, 161−174, 185−198, 251−253, 270−290
interaction 2	passive residues	309−310	123−141, 161−174, 185−198, 251−253, 270−290
interaction 2	passive residues	318−328	123−141, 161−174, 185−198, 251−253, 270−290
interaction 3	passive residues	358−368	123−141, 161−174, 185−198, 251−253, 270−290
interaction 4	passive residues	395−399	123−141, 161−174, 185−198, 251−253, 270−290
interaction 4	passive residues	423−428	123−141, 161−174, 185−198, 251−253, 270−290
interaction 5	passive residues	435−444	123−141, 161−174, 185−198, 251−253, 270−290
interaction 5	passive residues	465−472	123−141, 161−174, 185−198, 251−253, 270−290
interaction 5	passive residues	479	123−141, 161−174, 185−198, 251−253, 270−290
interaction 5	passive residues	483	123−141, 161−174, 185−198, 251−253, 270−290
interaction 5	passive residues	495−510	123−141, 161−174, 185−198, 251−253, 270−290
interaction 5	passive residues	513−519	123−141, 161−174, 185−198, 251−253, 270−290

Table 2. AIR Template for HADDOCK Simulations of Hsp90−p53 Complexes in Hsp90-C Binding Site

interaction	AIR template	Hsp90-M	P53
interaction 1	active residues	674−687	115−117, 136, 178, 182
interaction 2	active residues	674−687	242−245, 277−284, 288
interaction 1	passive residues		113, 114, 118−128, 134−141, 163, 173−184
interaction 2	passive residues		236, 238−241, 246−248, 273−278, 282−293

structures form with the relative solvent accessibility greater than 50% (Tables 1 and 2). Passive residues were defined as those within a 5 Å radius to the active residues and deemed as solvent accessible by the NACCESS program.[112] The AIR templates in Tables 1 and 2 define that that specific residues on the surface of the p53-DBD are expected to be in close vicinity of respectively specified group of Hsp90 residues during complex formation. These conditions are modeled using an ambiguous distance restraint between all atoms of the source residue to all atoms of the target residue that are assumed to be in the interface.[109−111]

Multiple HADDOCK runs (∼1000) were conducted to simulate binding of the ensemble of solution conformations of the p53-DBD with Hsp90. A large number of independent runs (with ∼2000 randomly generated initial structures in each of the runs) are expected to produce an adequate sampling of the conformational space for the Hsp90−cochaperone complexes. A HADDOCK protocol that allows protein docking with the conformational ensembles of multiple crystal structures of Hsp90 was also adopted in docking simulations. To mimic different conditions of the NMR experiments in which the p53-DBD was titrated with various constructs of Hsp90,[74] we explored ensemble-based docking with the multiple functional states of Hsp90 using three different set of AIR templates. The protein ensemble included a total of 500 representative snapshots taken from previously reported MD simulations[106] of the crystal structures of the full-length Hsp90 dimer. In addition, we supplemented MD-based ensemble of representative functional forms by extracting conformational states along the low frequency modes for each of the Hsp90 crystal structures. These soft modes may serve as additional indicators of large-scale functional motions determined by the equilibrium structure. We used the DC-ENM server[115] that utilizes the lowest normal modes from the GNM analysis of the crystal structures and distance constraints obtained from the NMR data.[74]

Experimentally guided docking simulations were run using three different sets of active residues involved in the Hsp90−p53 interactions: (a) active residues from both the Hsp90-M and Hsp90-C domains, (b) only a set of the Hsp90-M active residue, and (c) only a set of the Hsp90-C active residues. The details of the employed docking protocol were described in our recent study of the Hsp90−cochaperone binding.[107] In brief, the simulation procedure consists of three consecutive stages: (a) randomization of orientations followed by rigid body energy minimization (EM) and (b) semi-flexible simulated annealing in torsion angle space (TAD-SA), which consists of a rigid body MD search and first round of simulated annealing, followed by a second round semi-flexible simulated annealing during which side chains at the interface are free to move. (c) A third round of semi-flexible simulated annealing is the next step of the search during which both side chains and backbone at the interface are free to move. A final refinement in Cartesian space with explicit solvent concludes the run. During the first round of rigid body search and simulated annealing, docked solutions were judged by the HADDOCK score with standard weights of the individual contributions as defined in the following equation[111]

$$\text{HADDOCK Score} = E_{\text{vdw}} + E_{\text{elec}} + E_{\text{AIR}} \quad (1)$$

In this equation, E_{vdw} is the van der Waals energy, E_{elec} is the electrostatic energy, and E_{AIR} is the distance restraint contribution of AIRs. The best 200 docked models were submitted to cycles of the semi-flexible simulated annealing and final water refinement. During semi-flexible stages of the HADDOCK protocol, the intermolecular AIRs were combined with the intramolecular constraints that preserve the integrity of secondary structures. These intramolecular interactions were formatted into a distance restraint file and uploaded to HADDOCK as unambiguous interaction restraints. After the water refinement stage the HADDOCK score was calculated as the following weighted sum:[111]

$$\text{HADDOCK Score} = 1.0E_{\text{vdw}} + 0.2E_{\text{elec}} + 0.1E_{\text{dist}} + 1.0E_{\text{solv}} \quad (2)$$

dx.doi.org/10.1021/ci400434g | J. Chem. Inf. Model. 2013, 53, 2962−2978

where E_{solv} the solvation energy is term, and E_{dist} is the distance restraints energy contribution that includes both unambiguous interaction restraints and AIRs. The nonbonded intermolecular interactions were calculated with an 8.5 Å cutoff using the OPLS parameters. The dielectric constant epsilon was set to 10 in the vacuum part of the protocol and to 1 for the explicit solvent refinement. The secondary structure elements were kept intact during the simulated annealing refinement through hydrogen bond and dihedral angle restraints. The cutoff distance of 10 Å and a minimum cluster size of five structures were used in clustering of docked poses. The best scored structures from each cluster were reported as low-energy docked models. The root-mean-square deviation (RMSD) values were calculated based on the interface backbone atoms after superposition on the interface backbone atoms of the largest component of the cluster.

Structural Refinement of Docking Models. The low energy HADDOCK models were initially optimized using the 3Drefine method[116] that is based on an atomic-level energy minimization using a composite physics and knowledge-based force fields. This approach allows for a robust refinement of the global topology and local structural quality parameters including the hydrogen bond networks and side-chain interactions.[116] The optimized docked modes were then subjected to MD refinement simulations using NAMD[117,118] with the CHARMM27 force field[119,120] and implicit solvent calculations.[121] Finally, the average structures obtained from MD trajectories were optimized by the 3Drefine method at the last step. This protocol allows for a "self-consistent" iteration of global and local refinement of the docked models, assuring that the global topology and the side-chain interaction networks in the final structures are intrinsically consistent and relatively insensitive to the energy force field. The MD protocol is consistent with previous simulations of the Hsp90 crystal structures[106,107] and was described in detail in our recent studies.[122,123] Briefly, the system was subjected to initial minimization for 20,000 steps keeping the protein backbone fixed, which was followed by 20,000 steps of minimization without any constraints to allow system to relieve any steric contacts and relax freely. Equilibration was done in stages by gradually increasing the system temperature in steps of 20 K starting from 10 K until 310 K. At each stage, 30 ps equilibration was run using a restraint of 10 kcalmol^{-1} Å^{-2} on Cα atoms. The system was then equilibrated for 300 ps at 310 K using Langevin piston (NPT). After the restraints were removed, the system was equilibrated for 300 ps. A productive stage of the NPT simulation was then run on the equilibrated structure for 5 ns keeping the temperature at 310 K and pressure at 1 bar using Langevin piston coupling algorithm.

Coarse-Grained Modeling. Consistently with our earlier work,[106,107] we used the GNM representation of the protein structure to characterize global dynamics and functional motions of the Hsp90−p53 complexes. The systems are modeled as a network of N nodes identified by the α-carbon atoms where the fluctuations of each node are isotropic and Gaussian. The topology of the protein structure is described by N × N Kirchhoff matrix of inter-residue contacts, $\mathbf{\Gamma}$, where the off-diagonal elements are −1 if the nodes are within a cutoff distance r_c and zero otherwise. Bonded and nonbonded pairs of residues located within an interaction cutoff distance r_c = 7.0 Å are assumed to be connected by springs with a uniform spring constant γ. The normal modes are found by diagonalization of the Kirchhoff matrix $\mathbf{\Gamma} = \mathbf{U\Lambda U}^T$.

$$\langle \mathbf{\Delta R_i} \times \mathbf{\Delta R_j} \rangle = \frac{3k_BT}{\gamma}[\mathbf{\Gamma}^{-1}]_{ij} = \frac{3k_BT}{\gamma}[\mathbf{U\Lambda U^T}]_{ij} = \frac{3k_BT}{\gamma}\sum_{k=1}^{N-1}\lambda_k^{-1}[\mathbf{u_k u_k^T}]_{ij} \quad (3)$$

Here, $\mathbf{U}$ is a unitary matrix, $\mathbf{U}^T = \mathbf{U}^{-1}$ of the eigenvectors $\mathbf{u_k}$ of $\mathbf{\Gamma}$, and $\mathbf{\Lambda}$ is the diagonal matrix of eigenvalues λ_k.The elements of the kth eigenvector $\mathbf{u_k}$ describe the displacements of the residues along the kth mode coordinate, and the kth eigenvalue, λ_k, scales with the frequency of the kth mode, where $1 \le k \le N - 1$. The eigenvalues λ_k and eigenvectors $\mathbf{u_k}$ are obtained via the NomadRef server.[124] Additionally, NMA calculations and analysis of low frequency modes were conducted using the WEBnm@ approach[125] that uses only the mass-weighted Cα atoms of the protein. This approach utilized the approximate normal modes calculation method proven to be efficient and accurate in computations of low-frequency domain motions.[126] The root-mean-square fluctuations of a given residue are evaluated as a sum over the contributions of all modes. The fluctuation of the i^{th} atomic degree of freedom along the eigenvector $\mathbf{u_k}$ reflects the mobility of residue i in the kth mode.

$$\langle (\mathbf{\Delta R_i})^2 \rangle = \frac{3k_BT}{\gamma}\sum_{k=1}^{N-1}(\lambda_k^{-1}\mathbf{u_k u_k^T})_{ii} \quad (4)$$

where k_B is the Boltzmann's constant, the temperature T in the simulation is 300 K, and n is the number of normal modes included. The residue-based fluctuations and conformational mobility profiles were estimated using oGNM computation of structural dynamics.[93]

Protein Structure Network Analysis. The network analysis of the Hsp90−p53 docked complexes was conducted by generating graphs in which amino acid residues were considered as nodes connected by edges corresponding to the noncovalent interactions between them.[76−83] The noncovalent interactions between side chain atoms are included, and the interactions between sequence neighbors are ignored. The pair of residues with the interaction strength I_{ij} greater than a user-defined cutoff (I_{min}) are connected by edges and produce a protein structure network graph for a given interaction strength I_{min}. In accordance with the analyses of protein structures,[76,80] we considered any pair of residues to be connected if I_{min} was greater than 3.0%. The refined docked models entering the network analysis have optimized side-chain interactions that could ensure an adequate graph representation of the interaction connectivity. The analysis of the interaction networks was done using PSN parameters such as hubs, cliques, and communities.[76−83] The hubs are highly connected nodes in the network. If the total number of edges incident on the node (called the degree of a node) is at least 4, the node is identified as a hub. A k-clique is defined as a set of k nodes that are represented by the protein residues in which each node is connected to all the other nodes. We have used a community definition[76−83] according to which in a k-clique community two k-cliques share $k - 1$ or $k - 2$ nodes. The network cliques and communities were considered to be stable if they were present in the final refined structure of the complex and remained intact in more than 75% of the 500 representative simulation snapshots. The construction of protein structure graphs and

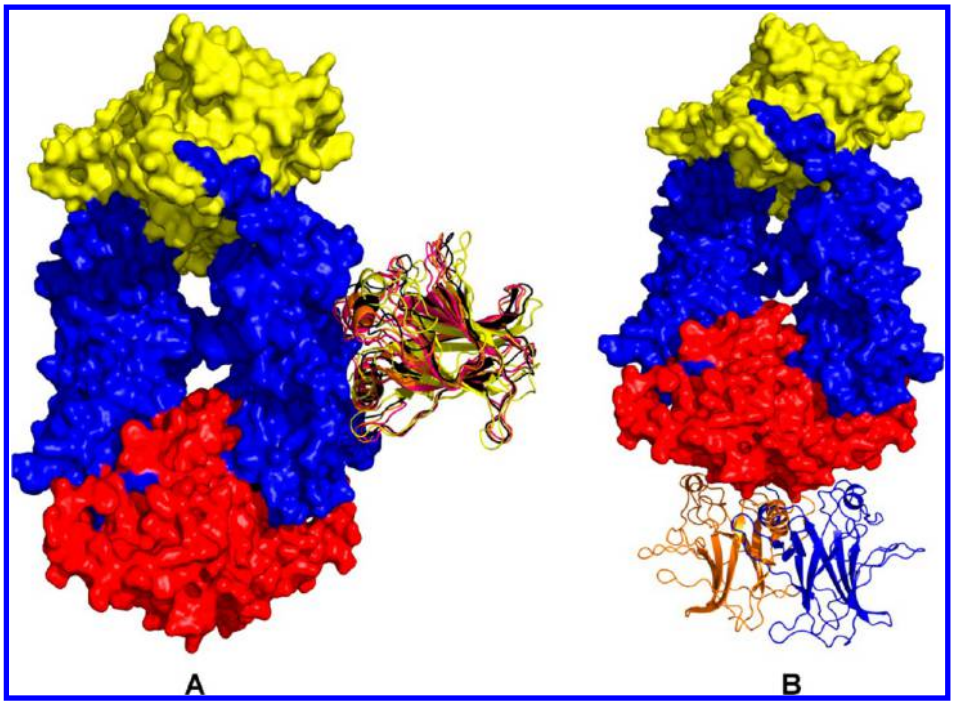

Figure 2. Predicted lowest energy clusters of the p53-DBD (ribbons) bound to the Hsp90-M domain (A) and Hsp90-C domain (B). Hsp90 is shown in a sphere-based protein representation with Hsp90-N in green, Hsp90-M in blue, and Hsp90-C in red. The cluster of low-energy docked solutions in the Hsp90-M domain (A) converged to a single binding mode. Two symmetry-related lowest energy docked models in the Hsp90-C domain are shown in orange and blue ribbons (B). Key interfacial contacts are mediated by the residues from the carboxy-terminal helix of the p53-DBD.

computation of the network parameters was done using a clique percolation method[127] as implemented in the CFinder program.[127,128]

RESULTS AND DISCUSSION

Structural Modeling of the Hsp90−p53 Interactions. By using protein docking and structural refinement of the predicted models, we reconstructed the recognition-competent states of the Hsp90−p53 complexes. Ensemble-based docking protocol with multiple Hsp90 conformations explored targeted and combined sets of active residues from the Hsp90-M and Hsp90-C domains. Probing binding preferences with structurally different forms of Hsp90 produced two persistent interaction modes of the p53-DBD formed with the closed Hsp90 dimer (Figure 2). Despite different sets of experimental restraints, HADDOCK simulations typically converged to the low-energy docked solutions assembled in the binding sites of the Hsp90-M (Figure 2A) and Hsp90-C domains (Figure 2B). A combined AIR set of active residues from both Hsp90-M and Hsp90-C domains allowed for a larger variability of the intermediate assemblies but resulted in a similar convergence to the two major binding modes. A single cluster of low-energy docked solutions was found in the Hsp90-M binding site (Figures 2A), whereas two symmetry-related low-energy solutions could be formed in the Hsp90-C interacting site (Figure 2B). The predicted binding modes suggested that key intermolecular contacts with the Hsp90-M and Hsp90-C domains could be provided by the same residues from the carboxy-terminal helix of the p53-DBD (residues 273−291). Consistent with the experimental data,[72−74] the primary interaction site is located near the DNA-binding surface of p53 and involves the interdomain region between the Hsp90-N and Hsp90-M domains. In this dominant binding mode the p53-DBD molecule is positioned in the middle of one Hsp90-M domain arm, projecting perpendicularly outward (Figure 2A).

The scatter graphs indicated a gradual improvement and consolidation of the intermolecular interface as the intermediate solutions converged to the binding modes in the Hsp90-M and Hsp90-C domains (Figures 3, 4). A more correlated region of the binding energy landscape was explored in docking simulations that converged to the Hsp90−p53 complex formed in the Hsp90-M domain (Figure 3). In this case, we observed an appreciable correlation (R = 0.67) between the HADDOCK scores and the interfacial RMSDs from the lowest energy structure. In this case, the dominant energy "funnel" could navigate most of the docking runs toward a single cluster of low-energy docked solutions (Figure 2A) that satisfy all active residue restraints in the Hsp90-M binding site. Docking simulations that converged to the alternative binding mode in the Hsp90-C domain reflected a greater degree of energetic and conformational variability, in part due to the greater flexibility of the C-terminal tail residues and the prevalence of electrostatic interactions in the interacting site (Figure 4). A weaker correlation between the HADDOCK scores and the interfacial RMSDs (R = 0.21) is exacerbated by a relatively small flow of conformations that could "descend" from the large cluster of intermediate states and reach the low-energy binding mode in the Hsp90-C domain (Figure 4). To summarize, experimentally guided protein docking and structural refinement have reconstructed dominant functional states of the Hsp90−p53 complexes. The final optimized conformations of the docked complexes (Text SI1, Supporting Information) are within RMSD = 0.35 Å from the MD-averaged structure for the primary binding mode in the Hsp90-M domain (Figure 3B) and within RMSD = 1.38 Å from the

dx.doi.org/10.1021/ci400434g | J. Chem. Inf. Model. 2013, 53, 2962−2978

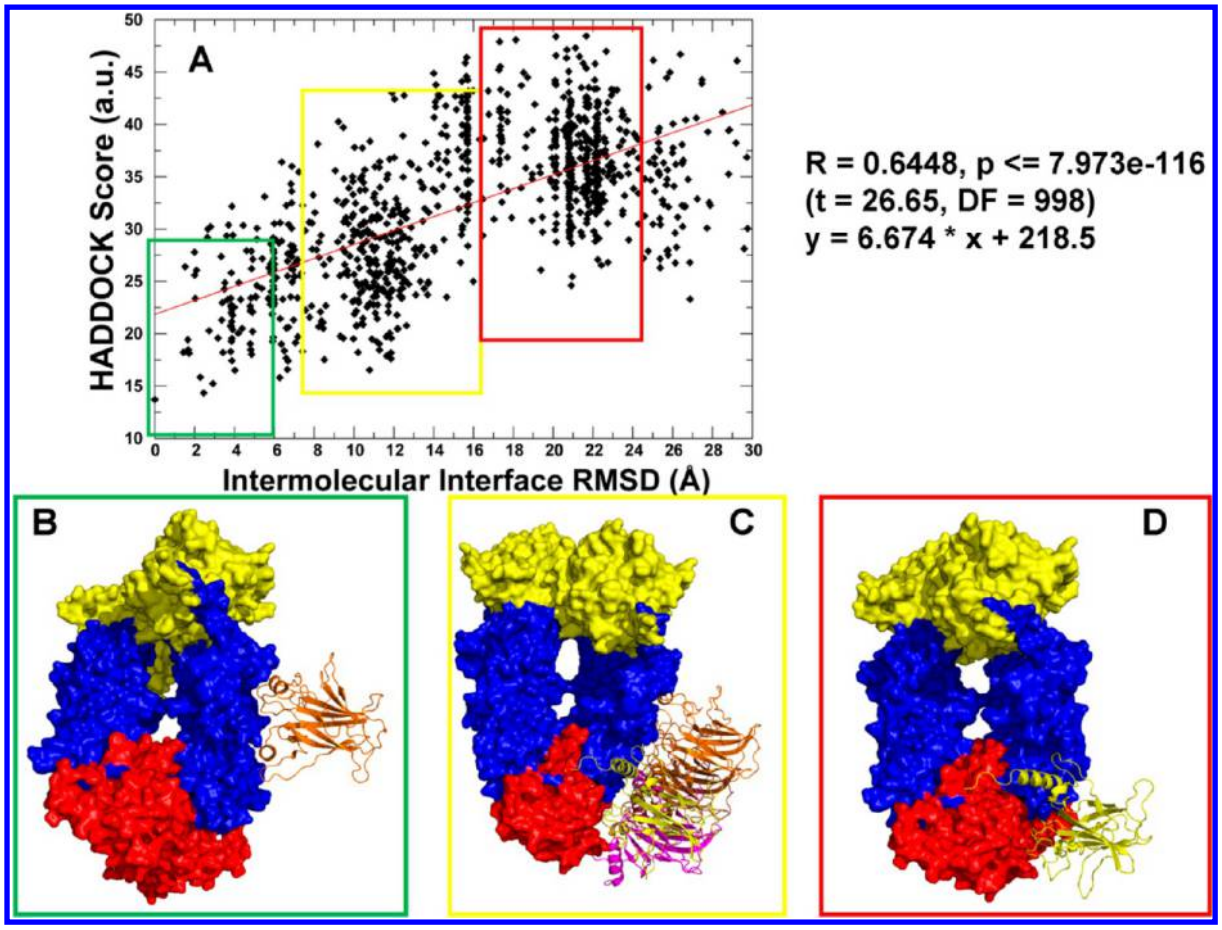

Figure 3. (A) Scatter graph of the docked solutions obtained using active residues from the Hsp90-M domain. The scatter graphs are based on HADDOCK scoring of the water-refined models. The intermolecular interface RMSD is based on residues forming the Hsp90−p53 interface in the Hsp90-M domain. The intermolecular contacts are defined based on the best HADDOCK model using a 5 Å cutoff. The multitude of intermediate states is divided into three major clusters: low-energy solutions (enclosed into a green rectangular) (B), intermediate states (enclosed into a blue rectangular) (C), and high energy states (enclosed into a red rectangular) (D). Hsp90 is shown in a sphere-based protein representation with Hsp90-N in green, Hsp90-M in blue, and Hsp90-C in red. Docked conformations of the p53-DBD are shown in ribbons.

MD-averaged conformation for the alternative binding mode in the Hsp90-C domain (Figure 4B). To establish connections with the NMR experiments and validate our predictions, we subjected the predicted models to a detailed structural analysis.

The binding interface in the Hsp90-M domain can be characterized by three major interacting clusters, where a central hydrophobic cluster is anchored by two clusters of hydrogen bonding interacting residues (Figures 5A,C). The hydrophobic component of the interacting site is formed by P303, L304, Y305, and V306 of Hsp90 that interact with the p53-DBD residues M243 and S240. The group of charged p53-DBD residues 174-RRCPHHER-181 forms a tight interacting cluster with the Hsp90-M residues 283-DITQEEYN-290 (Figure 5C). These Hsp90-M residues experienced significant chemical shift differences in NMR experiments.[74] The interacting p53 residues in the Hsp90-M domain are also involved in the p53-DBD interactions, including K120, S241, R248, R273, A276, C277, R280, and R283. Structural and functional studies of the p53-DNA binding[56−58] have established that the major groove contacts are mediated by the p53-DBD residues A276, C277, and R280 from the carboxy-terminal helix and K120 from the L1 loop, whereas R248 in the L3 loop is anchored to the DNA minor groove (Figure 1). A negatively charged region from the Hsp90-M domain that consists of residues E412, E415, E453, and D459 could closely mimic the major groove of DNA. The importance of this region was highlighted in the fluorescence polarization assays[74] where the charge alteration in the E412K and E415K mutants caused a considerable reduction in the Hsp90−p53 binding affinity. The binding interface between the p53-DBD and the Hsp90-M domain overlaps with the M−C interdomain hinge located at the "bottom" of a three-helix bundle (Figures 5A,C). According to our previous studies,[106,107] functional sites involved in allosteric interactions and client binding may be situated near the interdomain regions to control the interdomain communications and global motions of Hsp90. The interdomain residues interacting with the p53-DBD in the primary site of the Hsp90-M domain (Figure 5C) are closely positioned to the regulatory regions and overlap with the interacting sites of allosteric Hsp90 inhibitors.[103−105]

Structural Modeling of the Hsp90-C Interacting Site. The NMR studies have also implicated the Hsp90-C domain as another interacting site of the p53-DBD.[74] According to this study, Hsp90−p53 binding is mediated by a stretch of negatively charged residues within the C-terminal tail of Hsp90 and a cluster of positively charged residues in the helix 2 and L1 loop of the p53-DBD (Figure 1). Structural analysis of the Hsp90−p53 interactions in this site required remodeling of the C-tail residues (residues 679−689) that were unresolved in the crystal structure of the yeast Hsp90 dimer[22]

dx.doi.org/10.1021/ci400434g | J. Chem. Inf. Model. 2013, 53, 2962−2978

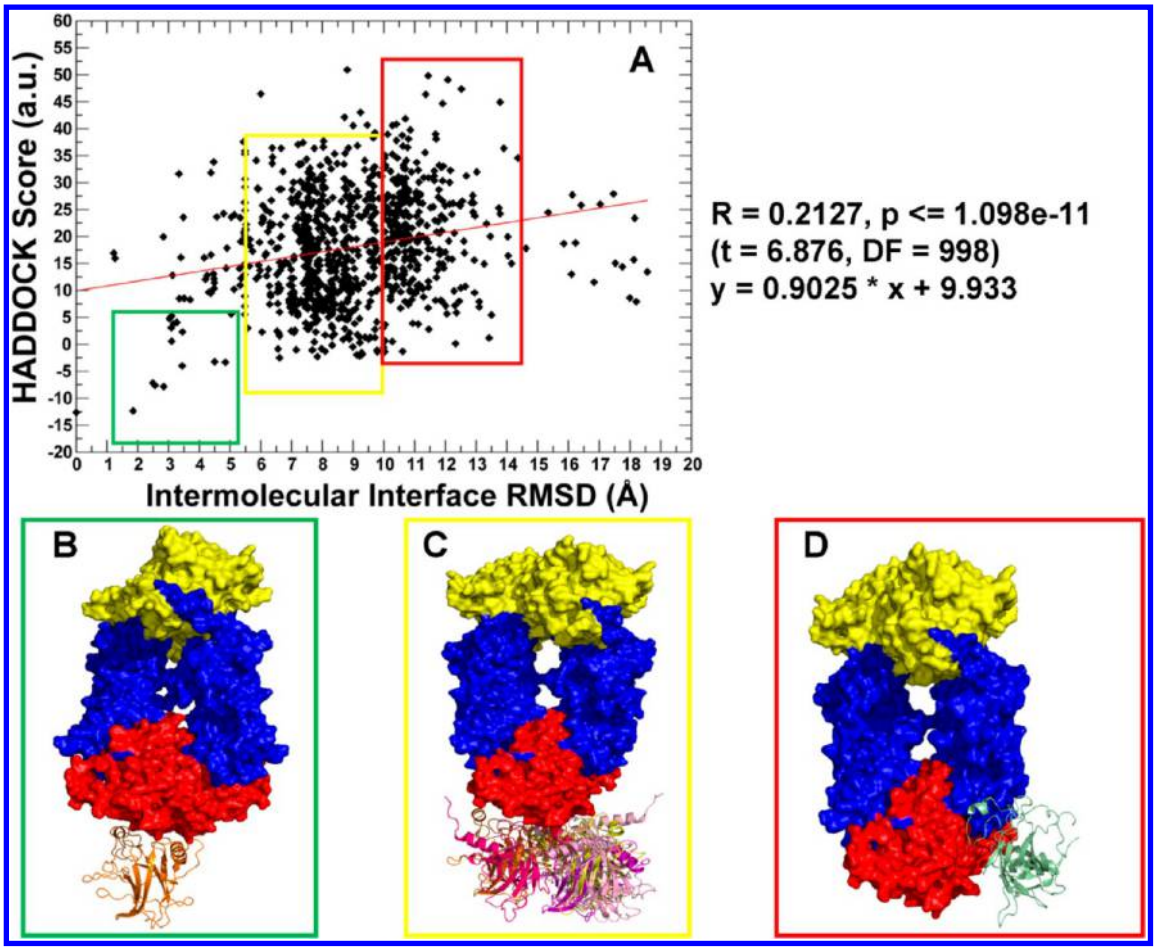

Figure 4. (A) Scatter graph of the docked solutions obtained using active residues only from the Hsp90-C domain. The scatter graphs are based on HADDOCK scoring of the water-refined models. The intermolecular interface RMSD is defined as in Figure 3. The multitude of intermediate states is divided into three major clusters: low-energy solutions (enclosed into a green rectangular) (B), intermediate states (enclosed into a blue rectangular) (C), and high energy states (enclosed into a red rectangular) (D). Hsp90 is shown in a sphere-based protein representation with Hsp90-N in green, Hsp90-M in blue, and Hsp90-C in red. Docked conformations of the p53-DBD are shown in ribbons.

but appeared to be important for p53 binding. In the fluorescence polarization titration assays,[74] these partially unstructured residues retained a considerable flexibility but became more ordered upon binding. We explored docking protocols using different sets of AIR templates, including a set of active residues from the Hsp90-C domain and a combined set of active residues from the Hsp90-M and Hsp90-C domains. In the docking runs, the p53 protein preferentially binds projecting outward from the C-terminal terminus and parallel to the "long arms" of the Hsp90 dimer (Figure 5B). Guided by a set of experimental restraints in the Hsp90-C binding site, the low energy docked conformations captured the fact that a stretch of five negatively charged residues 679-DEDEE-683 could largely determine the p53-DBD binding. In the predicted complex, the negatively charged residues E680, D681, E683, and E683 of the Hsp90-C tail became ordered and aligned against the K291 and N288 residues of the p53-DBD (Figure 5D). These polar interactions are supported by a network of hydrophobic interactions formed by L674, L676, and I678 of the Hsp90-M domain with C277, G279, and T284 of p53-DBD. The predicted structural models also reproduced the experimental mapping results.[74] The chemical shift perturbations in the p53-DBD were mainly observed in residues 277−293 (helix 2) and to a smaller extent in residues 113−125 from the L1 loop and residues 236−248 of the L3 loop (Figure 1). In accordance with these data, we found that residues 277−291 from the carboxy-terminal helix of the p53-DBD could mediate a network of primary intermolecular contacts with the Hsp90-C domain (Figures 5B,D). These residues are also central to the p53 interactions with the major groove of DNA.[56−58] A markedly smaller effect detected in the NMR experiments for residues 236−248 was reflected in our predictions as these residues were involved in direct interactions in the Hsp90-C binding site. The interacting residues were mapped closely to the regulatory motif that contains the "regulatory switch" residue A577 coordinating the interdomain communications. Notably, the p53-interacting hydrophobic cluster in the Hsp90-C domain (L674, L676, and I678) is directly linked to hydrophobic residues L652, F656, L658, and P661 that are implicated as hot spots in allosteric interaction networks and form putative interacting sites for allosteric C-terminal inhibitors of Hsp90.[103] In the biophysical experiments,[74] p53-DBD binding to the Hsp90-CTD induced a pronounced allosteric effect and chemical-shift perturbations in all three domains. A close proximity of the p53-DBD interacting residues to critical regulatory elements of the Hsp90-CTD could offer a plausible initial hypothesis that may be used to rationalize these observations. Consistent with these arguments, allosteric modulators of Hsp90 can weakly bind to the Hsp90-C domain and deplete mutated p53 client by interfering with the

dx.doi.org/10.1021/ci400434g | J. Chem. Inf. Model. 2013, 53, 2962−2978

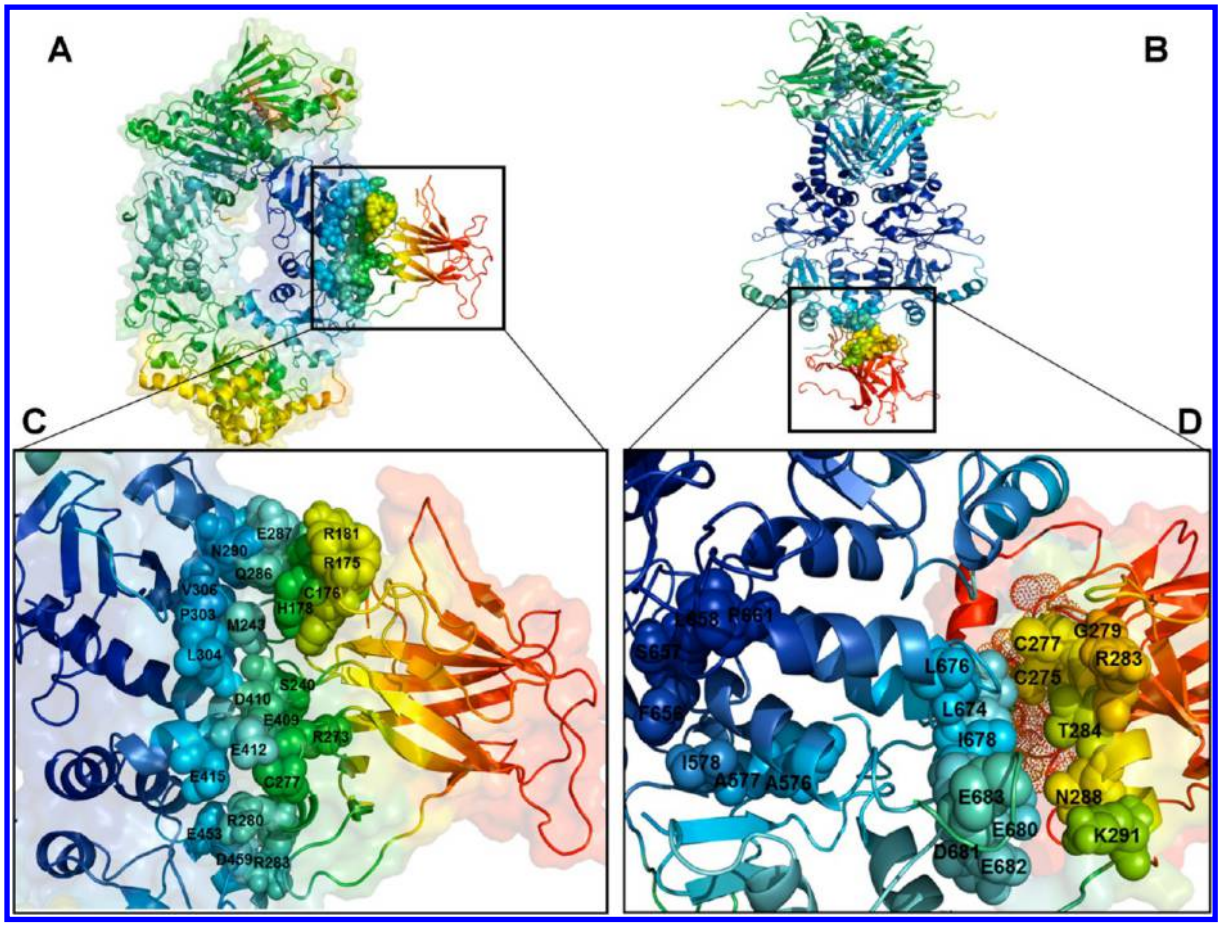

Figure 5. Structural prediction and analysis of the Hsp90−p53 binding sites. MD-refined docked models of the p53-DBD interacting sites at the Hsp90-M domain (A) and Hsp90-C domain (B). A close-up of the Hsp90−p53 interacting sites at the Hsp90-M domain (C) and Hsp90-C domain (D). The bound p53-DBD and a closed Hsp90 dimer are shown in ribbons colored according to the residue mobility. The color gradient from blue to red indicates the decreasing structural rigidity (or increasing conformational mobility) of protein residues. The structure of the Hsp90 dimer is enclosed in a 50% transparent molecular surface.

Hsp90 dimerization and destabilizing a chaperone complex.[103−105] Hence, the results of experimentally guided structural modeling reconstructed the main features of the binding interfaces in two major interacting sites. The refined structures of the Hsp90−p53 complexes could be further utilized in the protein structure network analysis to (a) assess energetics and structural stability of the Hsp90−p53 interactions and (b) identify functionally important hot spot residues.

Structurally Stable Interaction Networks. The graph-based network analysis evaluated the effect of p53 binding on structural stability of the regulatory complexes. We exploited the predicted structural models to identify key interaction networks and specific residues that stabilize the Hsp90−p53 complexes. To provide a comparison with structural and functional experiments of p53 binding with Hsp90 and DNA, we focused on the primary binding mode of the p53-DBD in the Hsp90-M domain. According to the primary conjecture of this model, the client-induced modulation of structural stability in the Hsp90−p53 complexes could be adequately described by variations in the PSN parameters. We observed that the 53-DBD binding resulted in an appreciable number of new communities formed at the intermolecular interface as well as at the interdomain Hsp90 regions (Figure 6A). Interestingly, there is also a significant increase in the number of hubs in the Hsp90−p53 complex that could reflect consolidation of the interfacial and intramolecular communities (Figure 6B). The interaction connectivity in the client-free Hsp90 dimer and the Hsp90−p53 complex could give rise to "small-world" networks[129,130] that are marked by a few highly connected and functionally critical hub nodes (Figure 6B). We found that the p53-DBD binding may result in a small separation of hubs from each other, i.e., a higher degree of interaction cooperativity. Thus, p53 binding may result in the overall strengthening of the global interaction network that is "tighter" than that of the client-free closed Hsp90 dimer. The p53-induced consolidation of the interdomain interactions between Hsp90-N and Hsp90-M domains may be inferred from the formation of new communities in Hsp90 such as F200−W277−Y344−V368, W277−R318−R347−D370, and L374−V345−N377 (Figure 6C,D). Of special interest is the emergence of the interfacial communities K426−D503−D506 and K307−E406−N247−R248−R249 that affect the stability of the interdomain between Hsp90-M and Hsp90-C (Figure 6D).

In this stable community, polar residues N247 and R248 from the p53-DBD binding site forms strong interactions with K307 and E406 from the intermodomain hinge of Hsp90. Another group of the interfacial communities (R444−L454−R280 and R463−D459−R283−R282) is formed near the interdomain region between Hsp90-M and Hsp90-C (Figure 6D). The formation of these communities assures structural stability of the Hsp90−p53 interface as well as the rigidity of

dx.doi.org/10.1021/ci400434g | J. Chem. Inf. Model. 2013, 53, 2962−2978

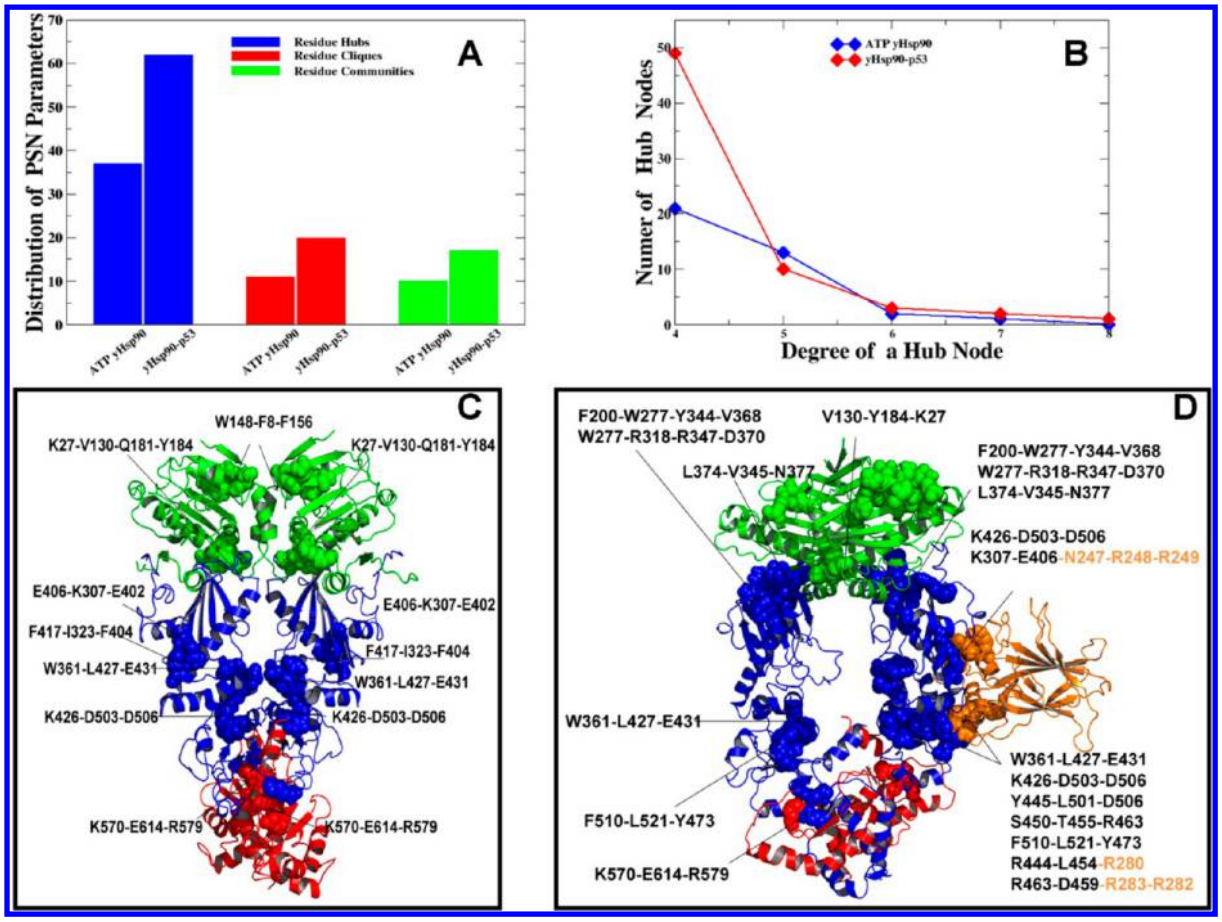

Figure 6. Network analysis of the Hsp90−p53 interactions in the Hsp90-M binding site. (A) Distribution of the PSN parameters in the Hsp90 dimer and Hsp90−p53 complex (hubs are shown in blue bars, cliques are in red bars, and communities are in green bars). (B) Relationship between the number of hub nodes and degree of a hub node. (C,D) Structural communities in the ATP-bound Hsp90 dimer and the Hsp90−p53 complex. Hsp90 is in ribbons colored according to the domain nomenclature: Hsp90-N in green, Hsp90-M in blue, and Hsp90-C in red. Hsp90 residues forming structural communities are shown in spheres colored according to the respective domains to which they belong. The p53-DBD residues that contribute to the interfacial communities are shown in orange spheres. Structural mapping of communities is indicated by arrows, and key communities are annotated with the p53 shown in orange.

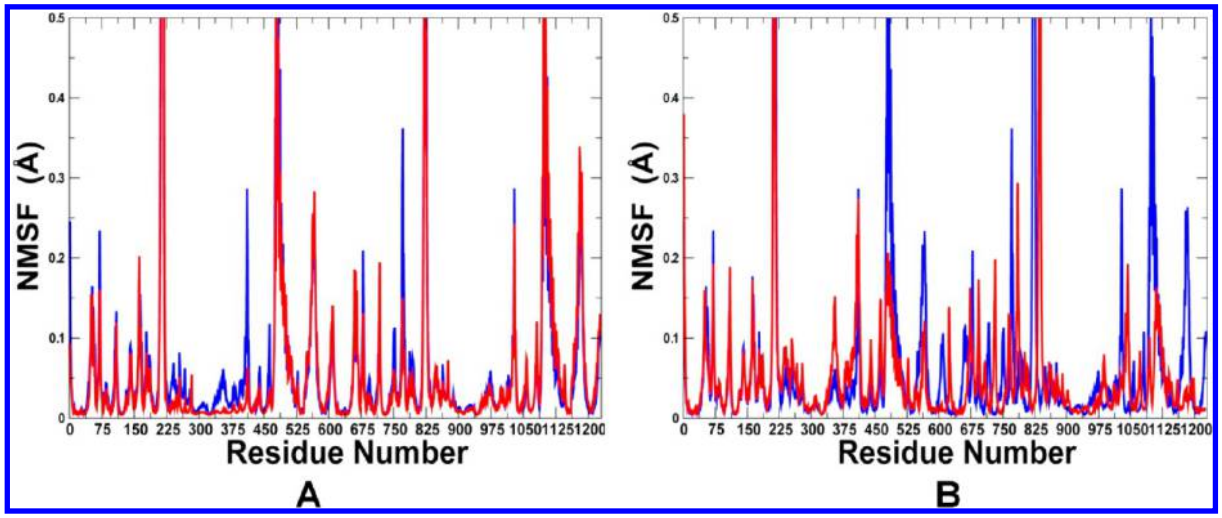

Figure 7. Residue-based NMSF profiles of Hsp90 from MD simulations. A comparative analysis of thermal fluctuations is presented for the unbound nucleotide-free Hsp90 in the closed form (blue) and predicted Hsp90−p53 complexes (red) for the Hsp90-M binding site (A, left panel) and in the Hsp90-C site (B, right panel). In monomer 1: Hsp90-N (residues 1−215), Hsp90-M (residues 216−471), and Hsp90-C (residues 472−609). In monomer 2: Hsp90-N (residues 610−824), Hsp90-M (residues 825−1089), and Hsp90-C (residues 1090−1227).

dx.doi.org/10.1021/ci400434g | J. Chem. Inf. Model. 2013, 53, 2962−2978

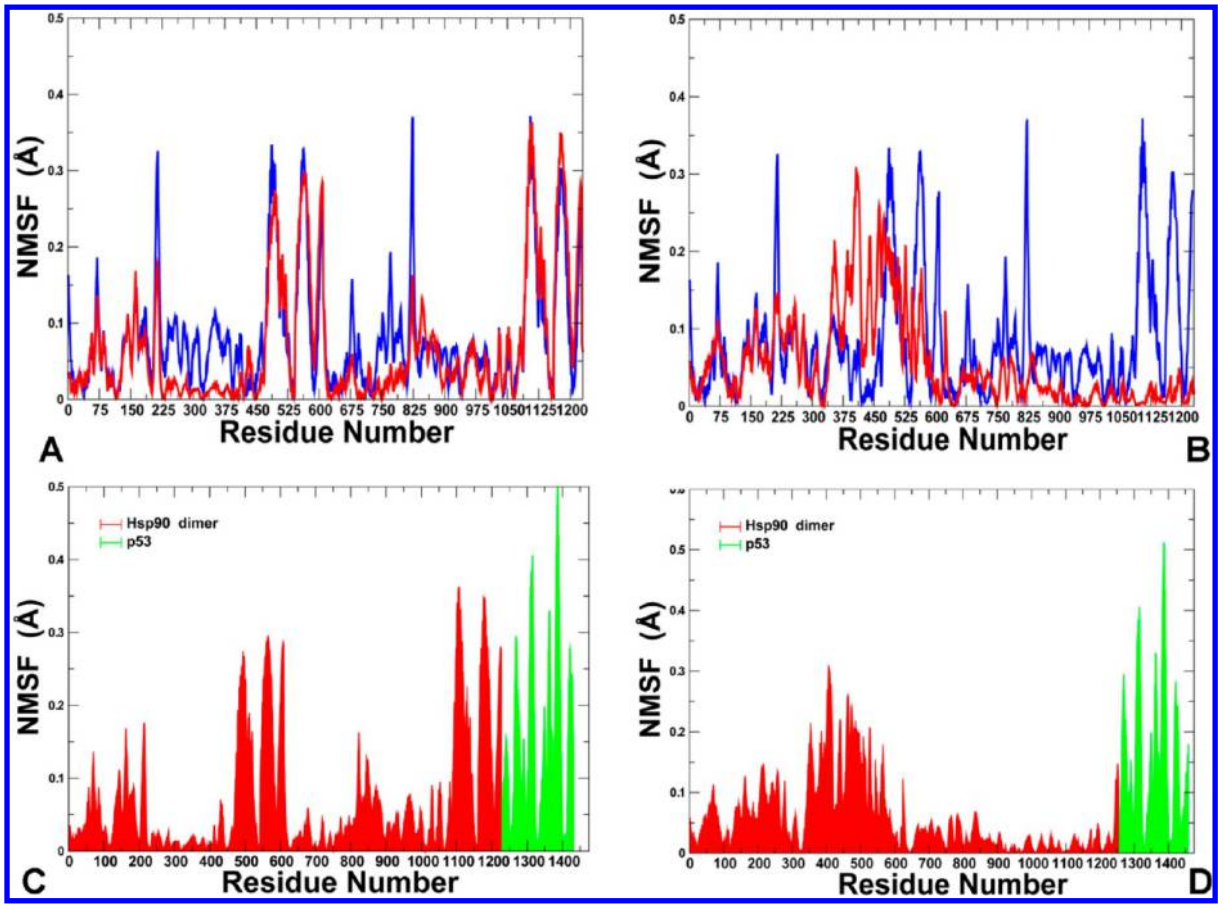

Figure 8. NMSF profiles of the Hsp90 residues were computed by averaging the residues fluctuations over three lowest frequency modes (C,D). NMSF profiles of the unbound Hsp90 (blue) and in the bound Hsp90 form (red) are shown for the predicted Hsp90−p53 complex at the Hsp90-M site (A,C) and the complex at the Hsp90-C interaction site (B,D). NMSF for the p53-DBD molecule (residues 1228−1431) are shown in green.

the interdomain regions in Hsp90. According to the PSN analysis, the key p53-DBD residues that form interfacial communities and may be responsible for structural stability of the Hsp90−p53 interactions include N247, R248, R280, and R283 (Figure 6D). In addition, the detected communities included supporting residues R249 and R282 that are not involved in direct interactions with Hsp90 but contribute to the overall stability of the network. Interestingly, R248, R280, and R283 are also critical for the interactions with DNA.[56−59] Furthermore, the importance of these residues for p53 function may be rather universal as oncogenic mutants in the p53-DBD include DNA-contact sites (R248Q, R248W, R273H, and R273C) and structural mutations (R175H, G245S, R249S, and R282W) that could affect structural integrity of the DNA-binding surface.[56,59]

Consistent with structural and functional experiments, the network analysis revealed that functionally important DNA-contact residues R248, R280, and R283 are also critical for structural stability of the Hsp90−p53 interactions. These residues are located in the dense protein regions and are supported by the interactions with R249 and R282 that are hot spots of structural mutations. The interdomain interactions play an important role in allosteric communications of protein systems.[84−90] Hence, the location of mediating p53 residues near the interdomain boundaries of Hsp90 could be intrinsically linked with the functional significance of these sites.

Client-Induced Modulation of Conformational Dynamics in the Hsp90 Chaperone. We analyzed MD equilibrium simulations of the two lowest energy models of the Hsp90−p53 complexes: the primary binding mode in the Hsp90-M domain and the alternative binding mode in the Hsp90-C domain. Conformational mobility of the Hsp90 residues was evaluated from these MD simulations by using the normalized mean square residue fluctuations (NMSF). This analysis revealed similar dynamics profiles in the unbound nucleotide-free Hsp90 and the p53 bound form of Hsp90 (Figure 7). However, client-induced modulation of conformational dynamics at different binding sites was evident in the Hsp90−p53 complexes. The reduced thermal fluctuations were observed at the binding interface of the Hsp90-M domain, including the N−M and M−C interdomain boundaries of the interacting monomer (Figure 7A). A more uniform moderation of conformational flexibility in Hsp90 could be seen as a result of p53 binding at the Hsp90-C binding site (Figure 7B). We then employed coarse-grained modeling of the two refined equilibrium structures of the Hsp90−p53 complexes in the Hsp90-M and Hsp90-C binding sites to characterize in details p53-induced changes in the global dynamics and functional motions of the Hsp90−p53 complexes. Several independent large scale studies have shown that ENM-based low frequency normal modes and principal components obtained from all-atom MD simulations are highly similar and evolutionary conserved.[97−99] Consequently, the normal modes can be adequately evaluated from the equilibrium structures of the Hsp90−p53 complexes using coarse-grained modeling approaches. First, to illustrate conformational diversity of Hsp90

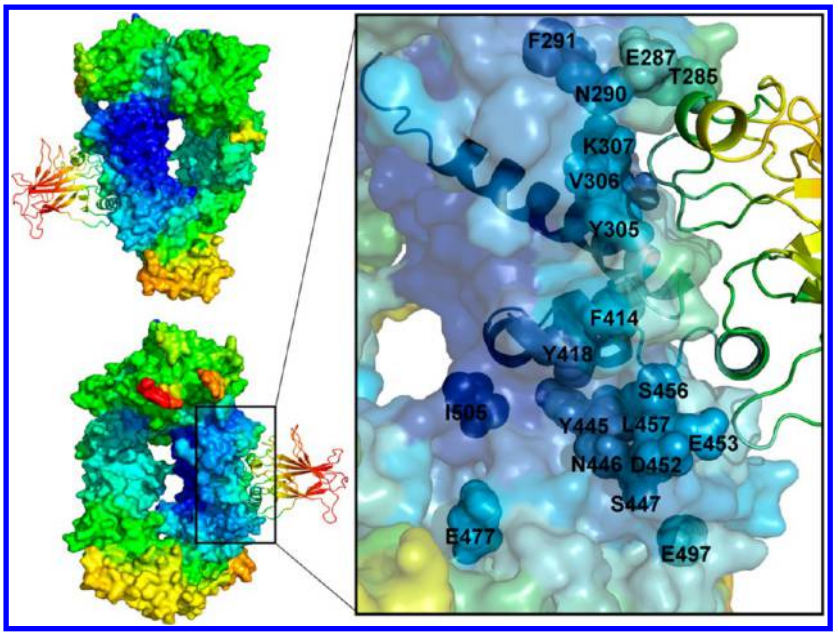

Figure 9. Conformational mobility mapping of the Hsp90−p53 complexes. The dynamic effect of p53 binding at the primary interacting site of the Hsp90-M was averaged over three lowest frequency modes. A surface-based Hsp90 representation and a ribbon representation of the p53-DBD are used. Coloring is according to the protein residue flexibility (color gradient from blue to red indicates the decreasing structural rigidity). The 180 degree global views of the Hsp90−p53 complex are shown on the left panel. A close-up of the Hsp90−p53 binding interface is shown on the right panel.

in different functional forms, we constructed GNM-based mobility maps of the Hsp90 crystal structures (Figure SI2, Supporting Information). Conformational mobility profiles of Hsp90 projected onto the low frequency modes indicated that the chaperone has a considerable degree of the inherent structural plasticity and binding of client proteins may incur considerable changes in the conformational equilibrium of Hsp90. To identify and characterize p53-induced changes in the functional motions of Hsp90, the equilibrium structures of the Hsp90−p53 complexes were subjected to the GNM analysis (Figure 8).

This analysis highlighted the role of the p53-DBD binding in strengthening structural rigidity of the interdomain Hsp90 regions. Indeed, the NMSF values were considerably reduced across the entire Hsp90-M domain of the interacting monomer, especially at the N−M and M−C interdomain boundaries (Figure 8A). According to this analysis, the N−M interdomain hinge (residues 374−LPLNLSREML−383) becomes uniformly rigid in the Hsp90−p53 complex. Similarly, structural proximity of the M−C hinge (residues 426−KLGVHE−431) also includes a number of allosterically affected residues (Figure 8A). The effect of the p53-DBD binding at the Hsp90-C site could be seen in partially suppressed fluctuations spread across multiple domains of the interacting monomer (monomer 2), while the other monomer may exhibit greater conformational changes along soft modes and determine functional motions of the complex (Figure 8B).

On the other hand, thermal fluctuations of the p53-DBD molecule remained rather large irrespective of the Hsp90 interaction site (Figure 8C,D). The NMSF values for the p53-DBD residues were on average considerably larger than the displacements of the Hsp90 residues and are comparable only to the most mobile elements of the Hsp90-C domain. This could indicate a significant degree of intrinsic flexibility in the p53-DBD during functional movements along soft low frequency modes. It is possible that conformational flexibility of p53 during binding with Hsp90 provides a mechanism for the ATP-stimulated subsequent release of the p53-DBD component and rapid dissociation of the short-lived Hsp90−p53 complexes.[69]

Allosteric Changes in Hsp90 Conformational Dynamics Are Confined to the p53-Interacting Monomer: Effect of Primary Interacting Site. We also compared the dynamic maps of the Hsp90−p53 complex with the NMR experiments[74] by focusing on residues that experienced significant chemical shift perturbations upon p53 binding. The p53-mediated chemical shift differences occurred primarily at a negatively charged surface region of the Hsp90-M domain, including residues 285−290, 305−307,407−419, and 445−459. The GNM-derived mobility maps revealed the character of functional movements and identified structurally stable regions of Hsp90 (Figure 9). The dynamic effect of p53 binding at the Hsp90-M interacting site could be seen in the enhanced structural rigidity of the interfaces that mimic p53-DNA interactions. The p53 residues from the helical segment within L2 loop (R175, C176, R181, H178, and M243) stabilize the Hsp90 residues 285−290 (T285, Q286, E287, N290, and F291). Additionally, the hydrophobic interactions of p53-M243 with P303, L304, and V306 from the Hsp90-M domain contribute to the improved stability of the regions that are proximal to the three-helix bundle (Figure 9). These interactions mimic the essential minor groove contacts formed by p53 in the complex with DNA.[56−58] The contacts mediated by R273, C277, R280, R283 from the carboxy-terminal helix of p53 can allosterically enhance structural rigidity in the Hsp90-M domain beyond the immediate interaction site. As a result, we observed p53-induced changes in conformational mobility of the F414, Y418, Y445, N446, S447, D452, E453, S456, and L457 residues in the Hsp90-M domain. This is consistent with the significant chemical shift perturbations observed in these

dx.doi.org/10.1021/ci400434g | J. Chem. Inf. Model. 2013, 53, 2962−2978

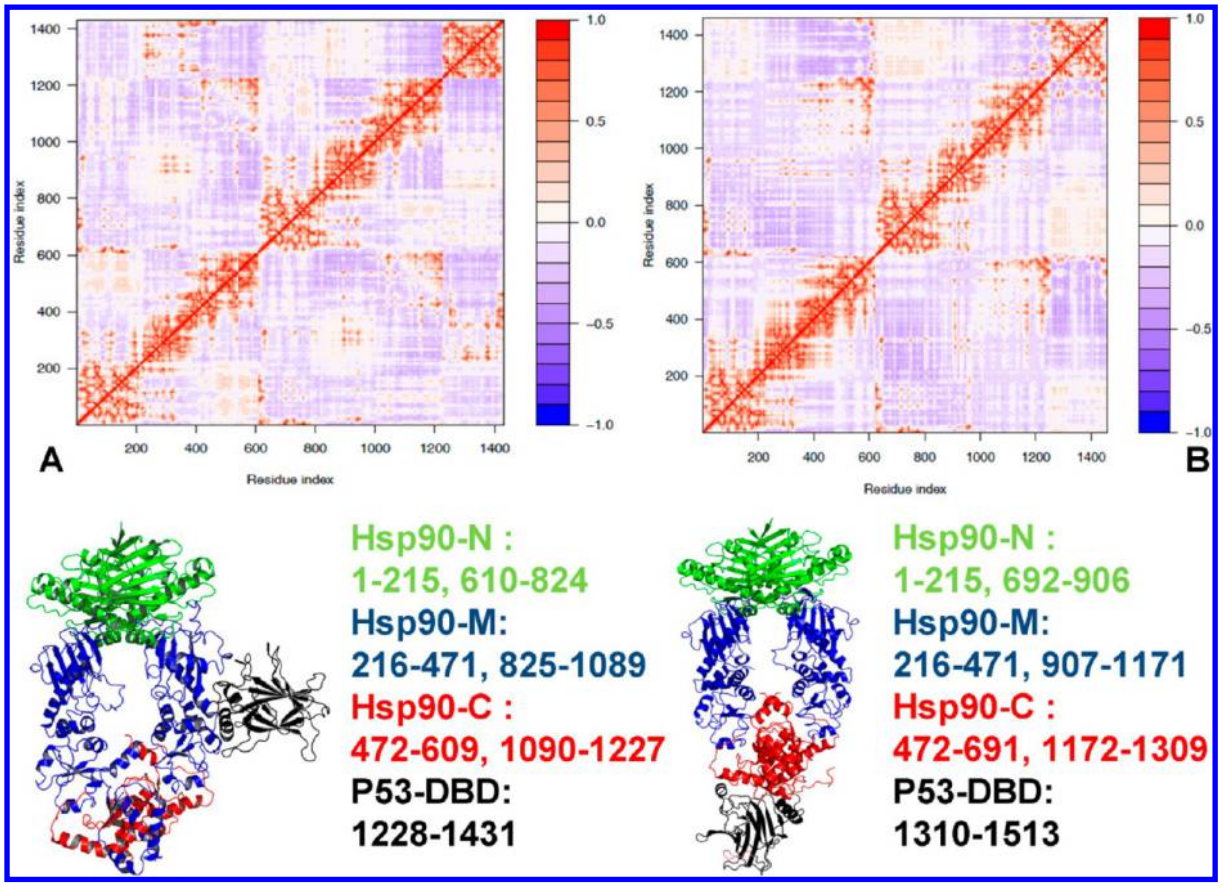

Figure 10. Analysis of correlated motions in the Hsp90−p53 complexes. The GNM-derived cross-correlation matrices of residue fluctuations are averaged over three low frequency modes in the Hsp90−p53 complex formed at the Hsp90-M site (A) and at the Hsp90-C site (B).

regions upon p53 binding.[74] Most of these residues overlap with the three-helix bundle that links the interdomain N−M and M−C regions and coordinates motions of the regulatory hinges (Figure 9). In general, the p53-mediated dynamic changes largely manifested in the increased rigidity of the interdomain N−M and M−C hinge regions of the interacting monomer (Figure 9). These residues overlap with the three-helix bundle that links the interdomain N−M and M−C regions and coordinates motions of the regulatory hinges.[106−108] Hence, we found that the variations in the functional dynamics profiles of the Hsp90−p53 complexes are consistent with the NMR studies. Structural modeling of the Hsp90−p53 binding is also consistent with the experimental evidence suggesting that the recognition sites of p53 are highly adaptable and capable of undergoing conformational changes upon binding. We observed that the fluctuations of the p53-DBD along low frequency modes are on average considerably larger than the movements of the chaperone residues. According to our results, a partial ordering of the p53 interacting residues may be coupled with structural plasticity of the β-sandwich (mostly red-colored residues) (Figure 9). These results are in accordance with the chemical shift changes within the p53-DBD that are largely concentrated at the DNA-binding interface (residues 125−144, 173−184, 235−245, and 277−293).[74] The β-sandwich core region is critical for p53 folding−unfolding, and the oncogenic potential of many β-sandwich mutations is closely associated with the low intrinsic stability of WT p53.[57−59] Despite some differences in the proposed mechanisms all NMR investigations have observed the disappearance of individual NMR signals for residues located within the β-sheet region of the p53-DBD.[70−74] It was concluded, however, that moderate structural changes, rather than extensive unfolding, may accompany binding of the p53-DBD to Hsp90.[74]

Effect of p53 Binding on Collective Movements of Hsp90 Chaperone. To characterize correlated motions and identify allosterically coupled regions in the Hsp90−p53 complexes, we also computed cross-correlation matrices of residue fluctuations along the low frequency modes. The allosteric effect of the p53-DBD binding in the Hsp90-M interacting site was quite moderate and mostly confined to the p53-interacting monomer (Figure 10A). We observed a reduction in positively correlated motions between the Hsp90-M domains of both monomers, which is a direct result of restricted motions near the binding site. Additionally, there was a modest decrease in the correlated motions of the Hsp90-N and Hsp90-C of the same monomer. A partial contraction in cooperative motions may be associated with the increased structural rigidity of the interacting monomer and a concomitant greater mobility of the second monomer (Figure 10A). Nonetheless, the dynamic fingerprint of the chaperone motions remained relatively similar in the Hsp90−p53 complex in comparison to the unbound nucleotide-free Hsp90 dimer.[106,107] The effect of the p53-DBD binding at the Hsp90-C site may have a more significant impact on collective motions (Figure 10B).

This is consistent with the strong allosteric effect of these interactions diffused across three domains as judged by the pattern of chemical shifts.[74] In particular, we observed a partial reversal in the character of concerted motions of the Hsp90-

dx.doi.org/10.1021/ci400434g | J. Chem. Inf. Model. 2013, 53, 2962−2978

MDs resulting in the anti-correlated movements (Figure 10B). The positive correlations between the Hsp90-N and Hsp90-C residues within the same monomer were partially depleted yielding to mostly anti-correlated fluctuations. Overall, p53 binding with the Hsp90-CTD could dampen positive correlated motions of the M-domains in different monomers as well as concerted intermonomer movements of the CTDs. This may compromise anti-correlated coupling between the NTD of one monomer and the CTD of the other monomer and impair opening−closing motions of the chaperone domains. However, the client-induced allosteric changes in Hsp90 dynamics are rather moderate and could not dramatically alter the pattern of collective motions of the molecular chaperone. Despite the overall similarity of the collective movements, the client binding at the C-terminal interaction site of Hsp90 may have a more significant impact on the chaperone dynamics, which is consistent with the stronger allosteric effect of these interactions revealed by the experimental studies. Although client-induced changes in the functional dynamics of the Hsp90−p53 complexes may be site-dependent, our results indicated that the Hsp90−p53 binding could promote conformational changes leading to the formation of the closed state of Hsp90. However, it is less unlikely that p53 binding can directly affect the kinetics of conformational transitions and the rate of ATP hydrolysis, which are typically regulated by such cochaperones as Aha1 and p23.[11−14,38−42] This analysis corroborates with the important experimental evidence that stimulation of the Hsp90−ATPase activity by the p53-DBD was possible only with a preformed complex between Hsp90 and the cochaperone Aha1.[74] According to our recent analysis Aha1 binding to Hsp90 could mediate significant changes in the collective motions and dynamical profile of Hsp90, catalyzing structural and dynamic changes in both monomers that contribute to the formation of a closed dimerized state.[107] Interestingly, the Aha1-NTD and p53-DBD binding target two nonoverlapping regions at the Hsp90-M domain, which may explain a synergistic effect of these proteins in accelerating conformational transitions of Hsp90 and stabilizing the structural arrangement of a closed dimer.

CONCLUSIONS

Integration of experimentally guided structural modeling and dynamics analysis was used to understand molecular mechanisms of the Hsp90−p53 interactions and allosteric regulation. Structural reconstruction of the Hsp90−p53 complexes and mapping of the client-induced dynamic changes enables identification of the functionally important residues in the binding sites. The variations in the functional dynamics profiles of the Hsp90−p53 complexes are consistent with the NMR studies and may explain differences in the functional role of the binding sites. We have shown that p53-induced changes in the global dynamics of Hsp90 can be allosterically transmitted beyond binding interfaces and affect the regulatory motifs of the Hsp90-M and Hsp90-C domains. At the same time, the intrinsic flexibility of p53-DBD could be preserved in the Hsp90−p53 complexes irrespective of the interaction site. The increased structural rigidity of the Hsp90−p53 complexes and reorganization of the structurally stable networks near the hinge regions and binding interfaces underlies the stimulatory effect role of p53 in stabilization of the closed Hsp90 dimer. Although binding of p53 could facilitate conformational changes leading to the formation of the closed state of Hsp90, it is less likely that the client protein would independently affect the rate of ATP hydrolysis, a function which is typically regulated by specific cochaperones. These results provide support to our conjecture that allosteric interactions, global motions, and client binding are often enabled by a small number of structurally conserved regulatory hotspots that could operate collectively during the ATPase cycle. Our study may also have important implications in structure-based design of allosteric modulators targeting the Hsp90 binding interfaces and selectively inhibiting therapeutically important client proteins.

ASSOCIATED CONTENT

Supporting Information

Coordinates of representative docking models for Hsp90−p53 complexes in the primary binding site are provided in the file Text SI1. The GNM-derived conformational mobility maps of the Hsp90 dimer crystal structures are presented in Figure SI2. This material is available free of charge via the Internet at http://pubs.acs.org.

AUTHOR INFORMATION

Corresponding Author

*Phone: 714-516-4586. Fax: 714-532-6048. E-mail: verkhivk@chapman.edu.

Notes

The authors declare no competing financial interest.

ACKNOWLEDGMENTS

This work was partly supported by institutional funding from Chapman University.

REFERENCES

(1) Pearl, L. H.; Prodromou, C. Structure, function, and mechanism of the Hsp90 molecular chaperone. *Adv. Protein Chem.* **2001**, *59*, 157−186.
(2) Richter, K.; Buchner, J. Hsp90: Chaperoning signal transduction. *J. Cell. Physiol.* **2001**, *188*, 281−290.
(3) Pearl, L. H.; Prodromou, C. Structure and mechanism of the Hsp90 molecular chaperone machinery. *Annu. Rev. Biochem.* **2006**, *75*, 271−294.
(4) Pearl, L. H.; Prodromou, C.; Workman, P. The Hsp90 molecular chaperone: An open and shut case for treatment. *Biochem. J.* **2008**, *410*, 439−453.
(5) Li, J.; Buchner, J. Structure, function and regulation of the hsp90 machinery. *Biomed. J.* **2013**, *36*, 106−117.
(6) Hanahan, D.; Weinberg, R. A. The hallmarks of cancer. *Cell* **2000**, *100*, 57−70.
(7) Zhao, R.; Davey, M.; Hsu, Y. C.; Kaplanek, P.; Tong, A.; Parsons, A. B.; Krogan, N.; Cagney, G.; Mai, D.; Greenblatt, J.; Boone, C.; Emili, A.; Houry, W. A. Navigating the chaperone network: An integrative map of physical and genetic interactions mediated by the Hsp90 chaperone. *Cell* **2005**, *120*, 715−727.
(8) McClellan, A. J.; Xia, Y.; Deutschbauer, A. M.; Davis, R. W.; Gerstein, M.; Frydman, J. Diverse cellular functions of the Hsp90 molecular chaperone uncovered using systems approaches. *Cell* **2007**, *131*, 121−135.
(9) Zhao, R.; Houry, W. A. Molecular interaction network of the Hsp90 chaperone system. *Adv. Exp. Med. Biol.* **2007**, *594*, 27−36.
(10) Taipale, M.; Jarosz, D. F.; Lindquist, S. Hsp90 at the hub of protein homeostasis: Emerging mechanistic insights. *Nat. Rev. Mol. Cell. Biol.* **2010**, *11*, 515−528.
(11) Prodromou, C. The 'active life' of Hsp90 complexes. *Biochim. Biophys. Acta* **2012**, *1823*, 614−623.
(12) Makhnevych, T.; Houry, W. A. The role of Hsp90 in protein complex assembly. *Biochim. Biophys. Acta* **2012**, *1823*, 674−682.

(13) Echtenkamp, F. J.; Freeman, B. C. Expanding the cellular molecular chaperone network through the ubiquitous cochaperones. *Biochim. Biophys. Acta* **2012**, *1823*, 668−673.
(14) Röhl, A.; Rohrberg, J.; Buchner, J. The chaperone Hsp90: changing partners for demanding clients. *Trends Biochem. Sci.* **2013**, *38*, 253−262.
(15) Workman, P.; Burrows, F.; Neckers, L.; Rosen, N. Drugging the cancer chaperone HSP90: combinatorial therapeutic exploitation of oncogene addiction and tumor stress. *Ann. N.Y. Acad. Sci.* **2007**, *1113*, 202−216.
(16) van Montfort, R. L.; Workman, P. Structure-based design of molecular cancer therapeutics. *Trends Biotechnol.* **2009**, *27*, 315−328.
(17) Travers, J.; Sharp, S.; Workman, P. HSP90 inhibition: Two-pronged exploitation of cancer dependencies. *Drug Discovery Today* **2012**, *17*, 242−252.
(18) Neckers, L.; Workman, P. Hsp90 molecular chaperone inhibitors: Are we there yet? *Clin. Cancer Res.* **2012**, *18*, 64−76.
(19) Krukenberg, K. A.; Street, T. O.; Lavery, L. A.; Agard, D. A. Conformational dynamics of the molecular chaperone Hsp90. *Q. Rev. Biophys.* **2011**, *44*, 229−255.
(20) Li, J.; Soroka, J.; Buchner, J. The Hsp90 chaperone machinery: Conformational dynamics and regulation by co-chaperones. *Biochim. Biophys. Acta* **2012**, *1823*, 624−635.
(21) Jackson, S. E. Hsp90: Structure and function. *Top. Curr. Chem.* **2013**, *328*, 155−240.
(22) Ali, M. M.; Roe, S. M.; Vaughan, C. K.; Meyer, P.; Panaretou, B.; Piper, P. W.; Prodromou, C.; Pearl, L. H. Crystal structure of an Hsp90-nucleotide-p23/Sba1 closed chaperone complex. *Nature* **2006**, *440*, 1013−1017.
(23) Shiau, A. K.; Harris, S. F.; Southworth, D. R.; Agard, D. A. Structural analysis of *E. coli* hsp90 reveals dramatic nucleotide-dependent conformational rearrangements. *Cell* **2006**, *127*, 329−340.
(24) Dollins, D. E.; Warren, J. J.; Immormino, R. M.; Gewirth, D. T. Structures of GRP94-nucleotide complexes reveal mechanistic differences between the hsp90 chaperones. *Mol. Cell* **2007**, *28*, 41−56.
(25) Krukenberg, K. A.; Forster, F.; Rice, L. M.; Sali, A.; Agard, D. A. Multiple conformations of *E. coli* Hsp90 in solution: insights into the conformational dynamics of Hsp90. *Structure* **2008**, *16*, 755−765.
(26) Krukenberg, K. A.; Southworth, D. R.; Street, T. O.; Agard, D. A. pH-dependent conformational changes in bacterial Hsp90 reveal a Grp94-like conformation at pH 6 that is highly active in suppression of citrate synthase aggregation. *J. Mol. Biol.* **2009**, *390*, 278−291.
(27) Graf, C.; Stankiewicz, M.; Kramer, G.; Mayer, M. P. Spatially and kinetically resolved changes in the conformational dynamics of the Hsp90 chaperone machine. *EMBO J.* **2009**, *28*, 602−613.
(28) Ratzke, C.; Mickler, M.; Hellenkamp, B.; Buchner, J.; Hugel, T. Dynamics of heat shock protein 90 C-terminal dimerization is an important part of its conformational cycle. *Proc. Natl. Acad. Sci. U.S.A.* **2010**, *107*, 16101−16106.
(29) Mickler, M.; Hessling, M.; Ratzke, C.; Buchner, J.; Hugel, T. The large conformational changes of Hsp90 are only weakly coupled to ATP hydrolysis. *Nat. Struct. Mol. Biol.* **2009**, *16*, 281−286.
(30) Ratzke, C.; Nguyen, M. N.; Mayer, M. P.; Hugel, T. From a ratchet mechanism to random fluctuations evolution of Hsp90's mechanochemical cycle. *J. Mol. Biol.* **2012**, *423*, 462−471.
(31) Ratzke, C.; Berkemeier, F.; Hugel, T. Heat shock protein 90's mechanochemical cycle is dominated by thermal fluctuations. *Proc. Natl. Acad. Sci. U.S.A.* **2012**, *109*, 161−166.
(32) Richter, K.; Muschler, P.; Hainzl, O.; Buchner, J. Coordinated ATP hydrolysis by the Hsp90 Dimer. *J. Biol. Chem.* **2001**, *276*, 33689−33696.
(33) McLaughlin, S. H.; Smith, H. W.; Jackson, S. E. Stimulation of the weak ATPase activity of human Hsp90 by a client protein. *J. Mol. Biol.* **2002**, *315*, 787−798.
(34) Siligardi, G.; Panaretou, B.; Meyer, P.; Singh, S.; Woolfson, D. N.; Piper, P. W.; Pearl, L. H.; Prodromou, C. Regulation of Hsp90 ATPase activity by the co-chaperone Cdc37p/p50cdc37. *J. Biol. Chem.* **2002**, *277*, 20151−20159.
(35) Siligardi, G.; Hu, B.; Panaretou, B.; Piper, P. W.; Pearl, L. H.; Prodromou, C. Co-chaperone regulation of conformational switching in the Hsp90 ATPase cycle. *J. Biol. Chem.* **2004**, *279*, 51989−51998.
(36) Panaretou, B.; Siligardi, G.; Meyer, P.; Maloney, A.; Sullivan, J. K.; Singh, S.; Millson, S. H.; Clarke, P. A.; Naaby-Hansen, S.; Stein, R.; Cramer, R.; Mollapour, M.; Workman, P.; Piper, P. W.; Pearl, L. H.; Prodromou, C. Activation of the ATPase activity of Hsp90 by the stress-regulated cochaperone Aha1. *Mol. Cell* **2002**, *10*, 1307−1318.
(37) Lotz, G. P.; Lin, H.; Harst, A.; Obermann, W. M. Aha1 binds to the middle domain of Hsp90, contributes to client protein activation, and stimulates the ATPase activity of the molecular chaperone. *J. Biol. Chem.* **2003**, *278*, 17228−17235.
(38) Meyer, P.; Prodromou, C.; Liao, C.; Hu, B.; Mark Roe, S.; Vaughan, C. K.; Vlasic, I.; Panaretou, B.; Piper, P W.; Pearl, L. H. Structural basis for recruitment of the ATPase activator Aha1 to the Hsp90 chaperone machinery. *EMBO J.* **2004**, *23*, 511−519.
(39) Meyer, P.; Prodromou, C.; Liao, C.; Hu, B.; Mark Roe, S.; Vaughan, C. K.; Vlasic, I.; Panaretou, B.; Piper, P W.; Pearl, L. H. Structural basis for recruitment of the ATPase activator Aha1 to the Hsp90 chaperone machinery. *EMBO J.* **2004**, *23*, 1402−1410.
(40) Retzlaff, M.; Hagn, F.; Mitschke, L.; Hessling, M.; Gugel, F.; Kessler, H.; Richter, K.; Buchner, J. Asymmetric activation of the Hsp90 dimer by its cochaperone Aha1. *Mol. Cell* **2010**, *37*, 344−354.
(41) Koulov, A. V.; Lapointe, P.; Lu, B.; Razvi, A.; Coppinger, J.; Dong, M. Q.; Matteson, J.; Laister, R.; Arrowsmith, C.; Yates, J. R., III; Balch, W. E. Biological and structural basis for Aha1 regulation of Hsp90 ATPase activity in maintaining proteostasis in the human disease cystic fibrosis. *Mol. Biol. Cell* **2010**, *21*, 871−884.
(42) Li, J.; Richter, K.; Reinstein, J.; Buchner, J. Integration of the accelerator Aha1 in the Hsp90 cochaperone cycle. *Nat. Struct. Mol. Biol.* **203**, *20*, 326−331.
(43) Street, T. O.; Lavery, L. A.; Agard, D. A. Substrate binding drives large-scale conformational changes in the Hsp90 molecular chaperone. *Mol. Cell* **2011**, *42*, 96−105.
(44) Motojima-Miyazaki, Y.; Yoshida, M.; Motojima, F. Ribosomal protein L2 associates with *E. coli*HtpG and activates its ATPase activity. *Biochem. Biophys. Res. Commun.* **2010**, *400*, 241−245.
(45) Falsone, S. F.; Kungl, A. J.; Rek, A.; Cappai, R.; Zangger, K. The molecular chaperone Hsp90 modulates intermediate steps of amyloid assembly of the Parkinson-related protein α-synuclein. *J. Biol. Chem.* **2009**, *284*, 31190−31199.
(46) Southworth, D. R.; Agard, D. A. Client-loading conformation of the Hsp90 molecular chaperone revealed in the cryo-EM structure of the human Hsp90:Hop complex. *Mol. Cell* **2011**, *42*, 771−781.
(47) Cunningham, C. N.; Southworth, D. R.; Krukenberg, K. A.; Agard, D. A. The conserved arginine 380 of Hsp90 is not a catalytic residue, but stabilizes the closed conformation required for ATP hydrolysis. *Protein Sci.* **2012**, *21*, 1162−1171.
(48) Street, T. O.; Lavery, L. A.; Verba, K. A.; Lee, C. T.; Mayer, M. P.; Agard, D. A. Cross-monomer substrate contacts reposition the Hsp90 N-terminal domain and prime the chaperone activity. *J. Mol. Biol.* **2012**, *415*, 3−15.
(49) Genest, O.; Reidy, M.; Street, T. O.; Hoskins, J. R.; Camberg, J. L.; Agard, D. A.; Masison, D. C.; Wickner, S. Uncovering a region of heat shock protein 90 important for client binding in E. coli and chaperone function in yeast. *Mol. Cell* **2013**, *49*, 464−473.
(50) Taipale, M.; Krykbaeva, I.; Koeva, M.; Kayatekin, C.; Westover, K. D.; Karras, G. I.; Lindquist, S. Quantitative analysis of HSP90-client interactions reveals principles of substrate recognition. *Cell* **2012**, *150*, 987−1001.
(51) Sharma, K.; Vabulas, R. M.; Macek, B.; Pinkert, S.; Cox, J.; Mann, M.; Hartl, F. U. Quantitative proteomics reveals that Hsp90 inhibition preferentially targets kinases and the DNA damage response. *Mol. Cell. Proteomics* **2012**, *11*, M111.014654.
(52) Wu, Z.; Moghaddas Gholami, A.; Kuster, B. Systematic identification of the Hsp90 candidate regulated proteome. *Mol. Cell. Proteomics* **2012**, *11*, M111.016675.
(53) Haupt, A.; Joberty, G.; Bantscheff, M.; Frohlich, H.; Stehr, H.; Schweiger, M. R.; Fischer, A.; Kerick, M.; Boerno, S. T.; Dahl, A.;

Lappe, M.; Lehrach, H.; Gonzalez, C.; Drewes, G.; Lange, B. M. Hsp90 inhibition differentially destabilises MAP kinase and TGF-β signalling components in cancer cells revealed by kinase-targeted chemoproteomics. *BMC Cancer* **2012**, *12*, 38.
(54) Samant, R. S.; Clarke, P. A.; Workman, P. The expanding proteome of the molecular chaperone HSP90. *Cell Cycle* **2012**, *11*, 1301−1308.
(55) Vogelstein, B.; Lane, D.; Levine, A. J. Surfing the p53 network. *Nature* **2000**, *408*, 307−310.
(56) Joerger, A. C.; Fersht, A. R. Structural biology of the tumor suppressor p53. *Annu. Rev. Biochem.* **2008**, *77*, 557−582.
(57) Bullock, A. N.; Henckel, J.; DeDecker, B. S.; Johnson, C. M.; Nikolova, P. V.; Proctor, M. R.; Lane, D. P.; Fersht, A. R. Thermodynamic stability of wild-type and mutant p53 core domain. *Proc. Natl. Acad. Sci. U.S.A.* **1997**, *94*, 14338−14342.
(58) Khoo, K. H.; Mayer, S.; Fersht, A. R. Effects of stability on the biological function of p53. *J. Biol. Chem.* **2009**, *284*, 30974−30980.
(59) Joerger, A. C.; Fersht, A. R. Structure-function-rescue: The diverse nature of common p53 cancer mutants. *Oncogene* **2007**, *26*, 2226−2242.
(60) Canadillas, J. M.; Tidow, H.; Freund, S. M.; Rutherford, T. J.; Ang, H. C.; Fersht, A. R. Solution structure of p53 core domain: Structural basis for its instability. *Proc. Natl. Acad. Sci. U.S.A.* **2006**, *103*, 2109−2114.
(61) Blagosklonny, M. V.; Toretsky, J.; Bohen, S.; Neckers, L. Mutant conformation of p53 translated in vitro or in vivo requires functional HSP90. *Proc. Natl. Acad. Sci. U.S.A.* **1996**, *93*, 8379−8383.
(62) Wang, C.; Chen, J. Phosphorylation and hsp90 binding mediate heat shock stabilization of p53. *J. Biol. Chem.* **2003**, *278*, 2066−2071.
(63) Whitesell, L.; Sutphin, P. D.; Pulcini, E. J.; Martinez, J. D.; Cook, P. H. The physical association of multiple molecular chaperone proteins with mutant p53 is altered by geldanamycin, an hsp90-binding agent. *Mol. Cell. Biol.* **1998**, *18*, 1517−1524.
(64) Walerych, D.; Kudla, G.; Gutkowska, M.; Wawrzynow, B.; Muller, L.; King, F. W.; Helwak, A.; Boros, J.; Zylicz, A.; Zylicz, M. *J. Biol. Chem.* **2004**, *279*, 48836−48845.
(65) Walerych, D.; Olszewski, M. B.; Gutkowska, M.; Helwak, A.; Zylicz, M.; Zylicz, A. *Oncogene* **2009**, *28*, 4284−4294.
(66) Müller, L.; Schaupp, A.; Walerych, D.; Wegele, H.; Buchner, J. Hsp90 regulates the activity of wild type p53 under physiological and elevated temperatures. *J. Biol. Chem.* **2004**, *279*, 48846−48854.
(67) Muller, P.; Ceskova, P.; Vojtesek, B. Hsp90 is essential for restoring cellular functions of temperature-sensitive P53 mutant protein but not for stabilization and activation of wild-type P53: Implications for cancer therapy. *J. Biol. Chem.* **2005**, *280*, 6682−6691.
(68) King, F. W.; Wawrzynow, A.; Höhfeld, J.; Zylicz, M. Co-chaperones Bag-1, Hop and Hsp40 regulate Hsc70 and Hsp90 interactions with wild-type or mutant p53. *EMBO J.* **2001**, 206297−206305.
(69) Walerych, D.; Gutkowska, M.; Klejman, M. P.; Wawrzynow, B.; Tracz, Z.; Wiech, M.; Zylicz, M.; Zylicz, A. ATP binding to Hsp90 is sufficient for effective chaperoning of P53 protein. *J. Biol. Chem.* **2010**, *285*, 32020−32028.
(70) Rüdiger, S.; Freund, S. M.; Veprintsev, D. B.; Fersht, A. R. CRINEPT-TROSY NMR reveals p53 core domain bound in an unfolded form to the chaperone Hsp90. *Proc. Natl. Acad. Sci. U.S.A.* **2002**, *99*, 11085−11090.
(71) Bom, A. P.; Freitas, M. S.; Moreira, F. S.; Ferraz, D.; Sanches, D.; Gomes, A. M.; Valente, A. P.; Cordeiro, Y.; Silva, J. L. The p53 core domain is a molten globule at low pH: Functional implications of a partially unfolded structure. *J. Biol. Chem.* **2010**, *285*, 2857−2866.
(72) Park, S. J.; Borin, B. N.; Martinez-Yamout, M. A.; Dyson, H. J. The client protein p53 adopts a molten globule-like state in the presence of Hsp90. *Nat. Struct. Mol. Biol.* **2011**, *18*, 537−541.
(73) Park, S. J.; Kostic, M.; Dyson, H. J. Dynamic interaction of Hsp90 with its client protein p53. *J. Mol. Biol.* **2011**, *411*, 158−173.
(74) Hagn, F.; Lagleder, S.; Retzlaff, M.; Rohrberg, J.; Demmer, O.; Richter, K.; Buchner, J.; Kessler, H. Structural analysis of the interaction between Hsp90 and the tumor suppressor protein p53. *Nat. Struct. Mol. Biol.* **2011**, *18*, 1086−1093.
(75) Vaughan, C. K.; Gohlke, U.; Sobott, F.; Good, V. M.; Ali, M. M.; Prodromou, C.; Robinson, C. V.; Saibil, H. R.; Pearl, L. H. Structure of an Hsp90-Cdc37-Cdk4 complex. *Mol. Cell* **2006**, *23*, 697−707.
(76) Brinda, K. V.; Vishveshwara, S. A network representation of protein structures: Implications for protein stability. *Biophys. J.* **2005**, *89*, 4159−4170.
(77) Ghosh, A.; Vishveshwara, S. A study of communication pathways in methionyl-tRNA synthetase by molecular dynamics simulations and structure network analysis. *Proc. Natl. Acad. Sci. U.S.A.* **2007**, *104*, 15711−15716.
(78) Ghosh, A.; Vishveshwara, S. Variations in clique and community patterns in protein structures during allosteric communication: investigation of dynamically equilibrated structures of methionyl tRNA synthetase complexes. *Biochemistry* **2008**, *47*, 11398−11407.
(79) Bhattacharyya, M.; Ghosh, A.; Hansia, P.; Vishveshwara, S. Allostery and conformational free energy changes in human tryptophanyl-tRNA synthetase from essential dynamics and structure networks. *Proteins* **2010**, *78*, 506−517.
(80) Vijayabaskar, M. S.; Vishveshwara, S. Interaction energy based protein structure networks. *Biophys. J.* **2010**, *99*, 3704−3715.
(81) Bhattacharyya, M.; Vishveshwara, S. Elucidation of the conformational free energy landscape in H.pylori LuxS and its implications to catalysis. *BMC Struct. Biol.* **2010**, *10*, 27.
(82) Sukhwal, A.; Bhattacharyya, M.; Vishveshwara, S. Network approach for capturing ligand-induced subtle global changes in protein structures. *Acta Crystallogr., Sect. D: Biol. Crystallogr.* **2011**, *67*, 429−439.
(83) Bhattacharyya, M.; Vishveshwara, S. Probing the allosteric mechanism in pyrrolysyl-tRNA synthetase using energy-weighted network formalism. *Biochemistry* **2011**, *50*, 6225−6236.
(84) Sethi, A.; Eargle, J.; Black, A. A.; Luthey-Schulten, Z. Dynamical networks in tRNA:protein complexes. *Proc. Natl. Acad. Sci. U.S.A.* **2009**, *106*, 6620−6625.
(85) Ghosh, A.; Sakaguchi, R.; Liu, C.; Vishveshwara, S.; Hou, Y. M. Allosteric communication in cysteinyl tRNA synthetase: a network of direct and indirect readout. *J. Biol. Chem.* **2011**, *286*, 37721−37731.
(86) Hansia, P.; Ghosh, A.; Vishveshwara, S. Ligand dependent intra and inter subunit communication in human tryptophanyl tRNA synthetase as deduced from the dynamics of structure networks. *Mol. Biosyst.* **2009**, *5*, 1860−1872.
(87) Rivalta, I.; Sultan, M. M.; Lee, N. S.; Manley, G. A.; Loria, J. P.; Batista, V. S. Allosteric pathways in imidazole glycerol phosphate synthase. *Proc. Natl. Acad. Sci. U.S.A.* **2012**, *109*, E1428−E1436.
(88) Vanwart, A. T.; Eargle, J.; Luthey-Schulten, Z.; Amaro, R. E. Exploring residue component contributions to dynamical network models of allostery. *J. Chem. Theory Comput.* **2012**, *8*, 2949−2961.
(89) Gasper, P. M.; Fuglestad, B.; Komives, E. A.; Markwick, P. R.; McCammon, J. A. Allosteric networks in thrombin distinguish procoagulant vs. anticoagulant activities. *Proc. Natl. Acad. Sci. U.S.A.* **2012**, *109*, 21216−21222.
(90) Miao, Y.; Nichols, S. E.; Gasper, P. M.; Metzger, V. T.; McCammon, J. A. Activation and dynamic network of the M2 muscarinic receptor. *Proc. Natl. Acad. Sci. U.S.A.* **2013**, *110*, 10982−10987.
(91) Bahar, I.; Lezon, T. R.; Yang, L. W.; Eyal, E. Global dynamics of proteins: Bridging between structure and function. *Annu. Rev. Biophys.* **2010**, *39*, 23−42.
(92) Haliloglu, T.; Bahar, I.; Erman, B. Gaussian dynamics of folded proteins. *Phys. Rev. Lett.* **1997**, *79*, 3090−3093.
(93) Yang, L. W.; Rader, A. J.; Liu, X.; Jursa, C. J.; Chen, S. C.; Karimi, H. A.; Bahar, I. oGNM: Online computation of structural dynamics using the Gaussian Network Model. *Nucleic Acids Res.* **2006**, *34*, W24−W31.
(94) Eyal, E.; Yang, L. W.; Bahar, I. Anisotropic network model: Systematic evaluation and a new web interface. *Bioinformatics* **2006**, *22*, 2619−2627.

(95) Ma, J. Usefulness and limitations of normal mode analysis in modeling dynamics of biomolecular complexes. *Structure* **2005**, *13*, 373−380.
(96) Bahar, I.; Rader, A. J. Coarse-grained normal mode analysis in structural biology. *Curr. Opin. Struc. Biol.* **2005**, *15*, 1−7.
(97) Keskin, O.; Jernigan, R. L.; Bahar, I. Proteins with similar architecture exhibit similar large-scale dynamic behavior. *Biophys. J.* **2000**, *78*, 2093−2106.
(98) Rueda, M.; Chacón, P.; Orozco, M. Thorough validation of protein normal mode analysis: a comparative study with essential dynamics. *Structure* **2007**, *15*, 565−575.
(99) Fuglebakk, E.; Echave, J.; Reuter, N. Measuring and comparing structural fluctuation patterns in large protein datasets. *Bioinformatics* **2012**, *28*, 2431−2440.
(100) Colombo, G.; Morra, G.; Meli, M.; Verkhivker, G. Understanding ligand-based modulation of the Hsp90 molecular chaperone dynamics at atomic resolution. *Proc. Natl. Acad. Sci. U.S.A.* **2008**, *105*, 7976−7981.
(101) Morra, G.; Verkhivker, G.; Colombo, G. Modeling signal propagation mechanisms and ligand-based conformational dynamics of the Hsp90 molecular chaperone full length dimer. *PLoS Comput. Biol.* **2009**, *5*, e1000323.
(102) Verkhivker, G. M.; Dixit, A.; Morra, G.; Colombo, G. Structural and computational biology of the molecular chaperone Hsp90: from understanding molecular mechanisms to computer-based inhibitor design. *Curr. Top. Med. Chem.* **2009**, *9*, 1369−1385.
(103) Morra, G.; Neves, M. A. C.; Plescia, C. J.; Tsutsumi, S.; Neckers, L.; Verkhivker, G. M.; Altieri, D. C.; Colombo, G. Dynamics-based discovery of allosteric inhibitors: Selection of new ligands for the C-terminal domain of Hsp90. *J. Chem. Theory Comput.* **2010**, *6*, 2978−2989.
(104) Matts, R. L.; Brandt, G. E.; Lu, Y.; Dixit, A.; Mollapour, M.; Wang, S.; Donnelly, A. C.; Neckers, L.; Verkhivker, G.; Blagg, B. S. A systematic protocol for the characterization of Hsp90 modulators. *Bioorg. Med. Chem.* **2011**, *19*, 684−692.
(105) Matts, R. L.; Dixit, A.; Peterson, L. B.; Sun, L.; Voruganti, S.; Kalyanaraman, P.; Hartson, S. D.; Verkhivker, G. M.; Blagg, B. S. Elucidation of the Hsp90 C-terminal inhibitor binding site. *ACS Chem. Biol.* **2011**, *6*, 800−807.
(106) Dixit, A.; Verkhivker, G. M. Probing molecular mechanisms of the Hsp90 chaperone: Biophysical modeling identifies key regulators of functional dynamics. *PLoS One* **2012**, *7*, e37605.
(107) Blacklock, K.; Verkhivker, G. M. Differential modulation of functional dynamics and allosteric interactions in the Hsp90-cochaperone complexes with p23 and Aha1: A computational study. *PLoS One* **2013**, *8*, e71936.
(108) Morra, G.; Potestio, R.; Micheletti, C.; Colombo, G. Corresponding functional dynamics across the Hsp90 Chaperone family: insights from a multiscale analysis of MD simulations. *PLoS Comput. Biol.* **2012**, *8*, e1002433.
(109) Dominguez, C.; Boelens, R.; Bonvin, A. M. HADDOCK: A protein−protein docking approach based on biochemical or biophysical information. *J. Am. Chem. Soc.* **2003**, *125*, 1731−1737.
(110) van Dijk, A. D.; Bonvin, A. M. Solvated docking: Introducing water into the modeling of biomolecular complexes. *Bioinformatics* **2006**, *22*, 2340−2347.
(111) van Dijk, A. D. J.; Kaptein, R.; Boelens, R.; Bonvin, A. M. J. J. Combining NMR relaxation with chemical shift perturbation data to drive protein−protein docking. *J. Biomol. NMR* **2006**, *34* (4), 237−244.
(112) Vriend, G. WHAT IF: A molecular modeling and drug design program. *J. Mol. Graph.* **1990**, *8*, 52−56.
(113) Wu, S.; Zhang, Y. LOMETS: A local meta-threading-server for protein structure prediction. *Nucleic Acids Res.* **2007**, *35*, 3375−3382.
(114) Wu, S.; Zhang, Y. MUSTER: Improving protein sequence profile-profile alignments by using multiple sources of structure information. *Proteins* **2008**, *72*, 547−556.
(115) Zheng, W.; Brooks, B. R. Modeling protein conformational changes by iterative fitting of distance constraints using reoriented normal modes. *Biophys. J.* **2006**, *90*, 4327−4336.
(116) Bhattacharya, D.; Cheng, J. 3Drefine: Consistent protein structure refinement by optimizing hydrogen bonding network and atomic-level energy minimization. *Proteins* **2013**, *81*, 119−131.
(117) Phillips, J. C.; Braun, R.; Wang, W.; Gumbart, J.; Tajkhorshid, E.; Villa, E.; Chipot, C.; Skeel, R. D.; Kalé, L.; Schulten, K. Scalable molecular dynamics with NAMD. *J. Comput. Chem.* **2005**, *26*, 1781−1802.
(118) Wang, Y.; Harrison, C. B.; Schulten, K.; McCammon, J. A. Implementation of accelerated molecular dynamics in NAMD. *Comput. Sci. Discov.* **2011**, *4*, 015002.
(119) MacKerell, A. D.; Bashford, D.; Bellott, M.; Dunbrack, R. L.; Evanseck, J. D.; Field, M. J.; Fischer, S.; Gao, J.; Guo, H.; Ha, S.; Joseph-McCarthy, D.; Kuchnir, L.; Kuczera, K.; Lau, F. T. K.; Mattos, C.; Michnick, S.; Ngo, T.; Nguyen, D. T.; Prodhom, B.; Reiher, W. E.; Roux, B.; Schlenkrich, M.; Smith, J. C.; Stote, R.; Straub, J.; Watanabe, M.; Wiórkiewicz-Kuczera, J.; Yin, D.; Karplus, M. All-atom empirical potential for molecular modeling and dynamics studies of proteins. *J. Phys. Chem. B* **1998**, *102*, 3586−3616.
(120) MacKerell, A. D., Jr.; Banavali, N.; Foloppe, N. Development and current status of the CHARMM force field for nucleic acids. *Biopolymers* **2001**, *56*, 257−265.
(121) Tanner, D. E.; Chan, K. Y.; Phillips, J. C.; Schulten, K. Parallel generalized Born implicit solvent calculations with NAMD. *J Chem. Theory Comput.* **2011**, *7*, 3635−3642.
(122) Dixit, A.; Verkhivker, G. Hierarchical modeling of activation mechanisms in the ABL and EGFR kinase domains: thermodynamic and mechanistic catalysts of kinase activation by cancer mutations. *PLoS Comput. Biol.* **2009**, *5*, e1000487.
(123) Dixit, A.; Verkhivker, G. Computational modeling of allosteric communication reveals organizing principles of mutation-induced signaling in ABL and EGFR kinases. *PLoS Comput. Biol.* **2011**, *7*, e1002179.
(124) Lindahl, E.; Azuara, C.; Koehl, P.; Delarue, M. NOMAD-Ref: Visualization, deformation and refinement of macromolecular structures based on all-atom normal mode analysis. *Nucleic Acids Res.* **2006**, *34*, W52−W56.
(125) Hollup, S. M.; Salensminde, G.; Reuter, N. WEBnm@: A web application for normal mode analyses of proteins. *BMC Bioinf.* **2005**, *6*, 52.
(126) Hinsen, K. Analysis of domain motions by approximate normal mode calculations. *Proteins* **1998**, *33*, 417−429.
(127) Palla, G.; Derényi, I.; Farkas, I.; Vicsek, T. Uncovering the overlapping community structure of complex networks in nature and society. *Nature* **2005**, *435*, 814.
(128) Adamcsek, B.; Palla, G.; Farkas, I.; Derényi, I.; Vicsek, T. CFinder: Locating cliques and overlapping modules in biological networks. *Bioinformatics* **2006**, *22*, 1021−1023.
(129) Vendruscolo, M.; Dokholyan, N. V.; Paci, E.; Karplus, M. Small-world view of the amino acids that play a key role in protein folding. *Phys. Rev. E: Stat., Nonlinear, Soft Matter Phys.* **2002**, *65*, 061910.
(130) Atilgan, A. R.; Akan, P.; Baysal, C. Small-world communication of residues and significance for protein dynamics. *Biophys. J.* **2004**, *86*, 85−91.